Published in final edited form as:

Dev Cell. 2020 February 24; 52(4): 477–491.e8. doi:10.1016/j.devcel.2020.01.036.

Tuba8 drives differentiation of cortical radial glia into apical intermediate progenitors by tuning modifications of tubulin C-termini

Susana I. Ramos[1], **Eugene V. Makeyev**[1], **Marcelo Salierno**[1], **Takashi Kodama**[3], **Yasuhiko Kawakami**[4], **Setsuko Sahara**[1,2,5,*]

[1]Centre for Developmental Neurobiology

[2]MRC Centre for Neurodevelopmental disorders, King's College London, New Hunt's House, Guy's Campus, London SE1s 1UL, United Kingdom

[3]Department of Otolaryngology-Head and Neck Surgery, The Johns Hopkins University School of Medicine, Baltimore, Maryland 21205

[4]Department of Genetics, Cell Biology and Development, Stem Cell Institute, Developmental Biology Center, University of Minnesota, Minneapolis, MN 55455

[5]Lead Contact

Summary

Most adult neurons and glia originate from radial glial progenitors (RGs), a type of stem cells typically extending from the apical to the basal side of developing cortex. Precise regulation of the choice between RG self-renewal and differentiation is critical for normal development, but the mechanisms underlying this transition remain elusive. We show that the non-canonical tubulin Tuba8, transiently expressed in cortical progenitors, drives differentiation of RGs into apical intermediate progenitors, a more restricted progenitor type lacking attachment to the basal lamina. This effect depends on the unique C-terminal sequence of Tuba8 that antagonizes tubulin tyrosination and Δ2-cleavage, two post-translational modifications (PTM) essential for RG fiber maintenance and the switch between direct and indirect neurogenesis and ultimately distinct neuronal lineage outcomes. Our work uncovers an instructive role of a developmentally regulated tubulin isotype in progenitor differentiation and provides new insights into biological functions of the cellular tubulin PTM "code".

Keywords

Cortical progenitor; radial glia; apical intermediate progenitor; cell fate; tubulin posttranslational modification; tyrosination; Δ2-tubulin

[*]**Correspondence:** setsuko.sahara@kcl.ac.uk.

AUTHOR CONTRIBUTIONS

S.I.R and S.S designed and performed all experiments, acquired and analyzed the data. M.S. helped live imaging analysis. S.I.R., E.M., and S.S wrote the manuscript. Y.K. characterized Fgf10-floxed and null mice, prepared samples and organized the Fgf10KO RNAseq analysis. E.M. analysed the RNAseq data. T.K. wrote all Fiji analysis programs.

COMPETING INTERESTS

The authors have no competing financial or non-financial interests related to this work.

Introduction

Distinct types of differentiated cells in multicellular eukaryotes emerge from divergent populations of proliferating progenitors (Bertet et al., 2014). How this progenitor diversity is generated remains a major unresolved question in developmental biology. It has been a subject of extensive research, especially in the context of the developing mammalian cortex (Greig et al., 2013; Lui et al., 2011; Taverna et al., 2014). Currently, cortical progenitors are classified according to the location of their cell body during mitosis, morphological polarity, and proliferative potential (Arai and Taverna, 2017; Taverna et al., 2014). While neuroepithelial cells (NEs) and radial glia progenitors (RGs) are highly polarized cells with apico-basal polarity, other types of progenitor lack either or both contacts with the apical and basal lamina. Outer/basal RGs, which are abundant in the gyrencephalic cortex, possess basal contacts but lack apical contacts (Fietz et al., 2010; Hansen et al., 2010; Reillo and Borrell, 2012). Apical intermediate progenitors (aIPs, also known as short neural progenitors, SNPs) maintain apical processes and have a short fiber that projects towards, but does not reach the basal lamina (Gal et al., 2006). Basal intermediate progenitors (bIPs) lose their attachments from both apical and basal surfaces (Englund et al., 2005).

Cortical aIPs have been identified as progenitors that share many features with RGs, but lack basal attachments (Gal et al., 2006). The biological importance of this cell type is only beginning to be unravelled, perhaps due to a lack of known markers other than the activity of Tubulin α−1 (pTα) and Blbp/Glast promoters (Gal et al., 2006). Recent evidence suggests that increasing the aIP population by randomizing the spindle orientation in mitotic RGs in ventral telencephalon (vTel), leads to a depletion of the adult stem cells (Falk et al., 2017). A fate-mapping study of aIP/bIPs in the lateral vTel traced their progeny lineage to subtypes of striosomal/matrix projection neurons and cortical interneurons (Kelly et al., 2018; Petros et al., 2015). Fate mapping studies performed at mid-corticogenesis suggest that aIPs are prone to generate neurons directly, bypassing the bIP “expansion” pool, which explains their tendency to generate deeper layer neurons (Stancik et al., 2010). aIPs have been shown to originate from RGs (Tyler and Haydar, 2013). Downregulation of the canonical Notch effector CBF1 converts pGlast+ cells to pTα+, suggesting that CBF signalling is required to maintain RG fate (Mizutani et al., 2007). However, the mechanism driving the transition from cortical RGs to aIPs is unknown.

Microtubules (MTs) are essential components of eukaryotic cytoskeleton composed of highly conserved α- and β- tubulin dimers. Pointing at special importance of these molecules in developing nervous system, mutations in five tubulins (Tuba1a, Tubb2ba, Tubb2b, Tubb3, and Tubb5) are known to be associated with severe brain malformations, referred to as “tubulinopathies” (Breuss et al., 2017; Chakraborti et al. 2016; Romaniello et al., 2018). Despite their high structural similarity, different members of the α or β families, or tubulin isotypes, may have specific biological functions. This is illustrated by the discovery of specialized roles of β−tubulin isoforms in Drosophila visual system and platelet biogenesis (Belvindrah et al., 2017; Hoyle et al., 2000; Lecine et al., 2000). Furthermore, specific tubulin isoforms have different effects on microtubule dynamics (Belvindrah et al., 2017; Pamula et al., 2016; Vemu et al., 2017).

The negatively charged C-terminal tails of tubulins are located outside of the MT lattice where they can form contacts with MT-interacting proteins. Tubulin C-termini are known to undergo evolutionarily conserved posttranslational modifications (PTMs) further increasing tubulin diversity. These include (poly)glutamination, tyrosination-detyrosination, glycylation, and limited proteolysis to form Δ2/3 variants (Gadadhar et al., 2017; Roll-Mecak, 2019). Tubulin PTMs provide selective cues for microtubule effectors and motor proteins (Gadadhar et al., 2017; Roll-Mecak, 2019). The emerging concept of the "tubulin code" (analogous to that of the "histone code") posits that tubulins do not simply function as uniform building blocks for the MT network, but rather provide distinct molecular cues that may be interpreted by various MT-binding and motor proteins (Gadadhar et al., 2017; Roll-Mecak, 2019). While some evidence highlight the importance of tubulin PTMs in neurogenesis and migration (Aillaud et al., 2017; Erck et al., 2005; Nieuwenhuis et al., 2017), possible roles of specific tubulin isotypes and PTMs in cell fate specification remain poorly understood.

Here, we show that the Tuba8 tubulin-α isotype is expressed transiently at the onset of cortical neurogenesis where it plays an instructive role in the differentiation of cortical RGs to aIPs. Induction of aIP fate by Tuba8 is mediated by PTMs at its C-terminus. Its phenylalanine (F) residue interferes with tyrosination signalling and induces aIP differentiation with a preference towards direct neurogenesis. Moreover, the Tuba8 C-terminus is immune to detyrosination and Δ2-cleavage, a tubulin modification promoting the formation of RG fibers characterized by basal membrane contacts, active integrin signalling, and a bias towards indirect neurogenesis. Our work uncovers an instructive role of a specific tubulin isotype in progenitor cell fate transitions and provides insight into the regulation and functional significance of the C-terminal "tubulin code" in the context of neuronal progenitor cell fate differentiation.

Results

Tuba8 is an Fgf10 target transiently upregulated at the onset of cortical neurogenesis

We have previously shown that the fibroblast growth factor Fgf10, which is transiently expressed in cortical progenitors, controls the timing of NE-RG transition (Sahara and O'Leary, 2009). Fgf10-null knockout (KO) mice exhibit delayed RG differentiation, resulting in subsequent delays in neurogenesis. We therefore hypothesized that downstream targets of the Fgf10 may contribute to the emergence of characteristic RG traits, including their ability to differentiate into more specialized progenitor cell types and ultimately neurons.

To identify these factors, we carried out two transcriptome-wide mRNA-sequencing experiments (Figure 1A, S1). Firstly, we analysed genes differentially expressed between wild-type (WT) and Fgf10KO cortices at embryonic day (E)11.5 when the differences of RG marker genes between Fgf10KO and control brains are the most prominent (Sahara and O'Leary, 2009). Secondly, we examined gene expression changes induced by injection of the Fgf10 protein into the forebrain ventricles, i.e. a recapitulation of the Fgf10 signalling topology, as this protein is expressed at the apical side of the developing cortex. Intersection

between these two comparisons identified 57 genes that consistently increased or decreased their expression in an Fgf10-dependent manner (1.6-fold change; p-value < 0.05, Table S1).

We further mined public databases (Mouse Genome Informatics and Allen Brain Atlas) to shortlist genes with relevant spatiotemporal expression patterns. Of the Fgf10 targets showing readily detectable expression between E11.5 and E14.5, we focused on the *Tuba8* gene previously linked with a neurodevelopmental disorder called polymicrogyria (Figure 1B; (Abdollahi et al., 2009)). RT-qPCR analysis of WT embryonic mouse cortices confirmed that Tuba8 expression peaks at E11.5, generally coinciding with the onset of neurogenesis (Figure 1C) (Gao et al., 2014). Our *in situ* hybridization analyses showed that Tuba8 is expressed in the early cortex between E10.5 to E11.5 and its expression is restricted to a subset of progenitors (Figure 1D–E"). Tuba8 mRNA is still detectable at E12.5 (Figure 1F–F"), but appears to be downregulated from E13.5 onwards (Figure 1G–H"). This expression pattern is generally consistent with possible role of Tuba8 in early cortical neurogenesis.

To test whether, similar to Fgf10, Tuba8 might control the transition of NEs to RGs, we examined the expression of RG markers in KO mice where the Tuba8 coding sequence was interrupted by a 480-bp deletion in exon 2 (The Jackson Laboratory. 2012). However, we did not see a significant difference in the intensity of either RG marker, Blbp and Glast at the onset of RG differentiation (Figure S2A–I). We also quantified the Blbp transcript levels by RT-qPCR (Figure S2K). The expression levels of Blbp by E12.5 was indistinguishable between Tuba8KO and the WT. However, Tuba8KO cortices expressed significantly more Blbp at later stages of development, suggesting that Tuba8 is not involved in the NE-RG transition but instead controls differentiation of RGs into other cell types.

Tuba8 drives differentiation of RGs into aIPs

To gain insights into the biological function of Tuba8 in vivo, we firstly overexpressed Venus-tagged Tuba8 in cortical progenitors (Figure 2A, B). Control progenitors overexpressing GFP alone exhibited a fluorescent signal that was distributed throughout the cell, including the cell body and the apical and basal RG fibers (Figure 2B). Surprisingly, the Venus-Tuba8 signal localized to the cell body and apical radial fibers but was typically undetectable in the basal RG fiber in the cortical plate (Figure 2B). Progenitors showing this phenotype tended to extend thin multipolar fibers or to lack fibers altogether. In a few examples where Venus-Tuba8-expressing progenitors had basal processes, they also possessed elongated endfeet found at the border between the cortical plate (CP) and the ventricular zones. Finally, in cases where fibers reached the basal lamina, they often had highly branched protrusions (Figure 2B). These phenotypes raise two possibilities: (1) Tuba8 may be sequestered to the apical processes of RGs, through a mechanism reminiscent of the exclusion of Tpx2 from basal processes (Kosodo et al., 2011); (2) Tuba8 overexpression may induce a shorter basal RG processes, a hallmark of aIP cell morphology.

There are currently no known marker genes for aIPs and a combined expression profile of reporter constructs has been used to distinguish aIPs from RGs. The Blbp and Glast promoters are known to be upregulated in RGs, but downregulated in aIPs. On the other hand, pTα promoter is active in RGs, aIPs, and postmitotic neurons (Figure 2C; (Tyler and Haydar, 2013)). To examine whether Tuba8 promoted aIP fate in vivo, we overexpressed

pBlbp and pTα reporters at E11.5 when endogenous Tuba8 expression is the highest, together with Tuba8 overexpression or Tuba8 knockdown (Tuba8-miR-RNAi) constructs, or on their own into Tuba8KO cortices (Figure 2C–I). In controls, ~30% of progenitors in the VZ were pBlbp single-positive, α50% pBlbp/pTα double-positive, and ~15% pTα single-positive 24 hours post-electroporation (Figure 2E–E”’, I). In contrast, overexpression of Tuba8 significantly increased the percentage of pTα+ cells at the expense of both the pBlbp + and pBlbp+/pTα+ populations (Figure 2F–F”’, I). Conversely, electroporation of a knockdown construct or analysis of Tuba8KO cortices showed a significant reduction in the proportion of pTα+ cells in comparison to controls (Figure 2G–H”’, I), implying that Tuba8 may stimulate differentiation of RGs into aIPs.

RGs can be distinguished from aIPs by the presence of long basal processes. We therefore counted the number of cells with RG fibers contacting the basal lamina as a percentage of the total number of electroporated cells labelled by pCAG-H2BBFP in the VZ (Figure 2E–N). In control cortices, some electroporated progenitors showed RG-like long-basal-fiber morphology, whereas Tuba8-electroporated cortices had significantly fewer cells of this type (Figure 2J–K”’, N). In contrast, both knockdown and knockout of Tuba8 increased RG abundance (Figures 2L–M”’, N). These data support the hypothesis that Tuba8 promotes differentiation of RGs into aIPs. Interestingly, all fibers were either pBlbp+ or pBlbp/pTα+. No pTα single-positive fibers were detected, lending further support to this conclusion.

Since our pTα construct contained the Tubulin α1 promoter region, we wanted to rule out the possibility that the effects of Tuba8 were due to a genetic interaction with this sequence. We labelled cortical progenitors by pCAG-GFP and traced their fibers (Figure 2O–T). Overexpression of Tuba8 generated more short-fiber progenitors whose RG fibers terminate either in the VZ or CP (Figure 2P–Q’, T), whereas its knockdown and knockout increased the incidence of long-fiber progenitors extending their RG fibers to the basal lamina (Figure R–S’ and T) as compared to controls (Figure 2P, P’, T). Taken together, these data strongly suggest that Tuba8 promotes aIP differentiation from RGs in the developing mouse cortex.

A previous study estimated that aIPs account for 40-60% of the total progenitor pool between E13.5 and E16.5 (Gal et al., 2006). However, as described above, Tuba8 expression peaks transiently at E11.5 and diminishes by E13.5, a stage at which aIPs comprise a large fraction of the progenitor pool. It is therefore possible that Tuba8 contributes to aIP differentiation during early neurogenesis, leaving other players to regulate later stages. Alternatively, the effects of the Tuba8 protein might be sustained even after transcriptional downregulation of its encoding gene; perhaps as a result of the extremely long half-life of tubulin monomers (>50 hours; (Caron et al., 1985). To test whether the loss of Tuba8 induces a higher fraction of RGs, we introduced pBlbp and pTα reporter constructs into E13.5 Tuba8KO and WT cortices and quantified the number of RG fibers attached to the basal lamina in the CP 24 hours later (Figure S3A–H). We observed significantly more RG fibers in the Tuba8KO than in the WT (Figure S3H). We also confirmed this finding by counting RG fibers positive for the RG-specific marker RC2, and found a 26% increase in the Tuba8KO (Figure S3I–N’) while the total progenitor pool of Pax6+ cells in the VZ did not change between the WT and KO (Figure S3I, I’). Together, these data indicate that the loss of Tuba8 causes a long-lasting effect on RG/aIP transition.

Since randomizing cleavage planes of dividing cells by the manipulation of Insc or Lgn is known to increase the aIP population in vTel (Falk et al., 2017), we wondered whether Tuba8-induced aIP induction might be mediated in this manner. However, we did not detect a significant difference in orientation of mitotic spindles between the controls and Tuba8KO cortices (Figure S4).

Tuba8 promotes direct neurogenesis in the developing mouse cortex

Another important feature of aIPs is that they are biased towards direct neurogenesis and tend to bypass bIP production (Petros et al., 2015; Tyler and Haydar, 2013) (Figure 3A). To test whether the supernumerary long-fiber progenitors observed in Tuba8KO cortices could generate bIPs, we examined the frequency of direct/indirect neurogenesis by following the fate of progenitors after Tuba8 overexpression, knockdown, or knockout at E11.5 (Figure 3B–E). We analysed the distribution of H2BBFP+ cells 24 hours post-electroporation and performed co-immunostaining with a bIP marker, Tbr2, and a deep-layer marker, Ctip2 to estimate the fractions of cells, which remain in the proliferative VZ, and those that differentiate into bIPs or neurons (Arlotta et al., 2005; Chen et al., 2008; Englund et al., 2005). We used Ctip2 as a cortical neuronal marker instead of Tbr1 (Cárdenas et al., 2018; Laguesse et al., 2015; Vitali et al., 2018), because it encompasses Tbr1 population, labels more neurons, and does not co-localize with proliferative markers such as phospho-histone H3 and Ki67 (Figure S5A–F”). In controls, 61% of electroporated cells remained in the VZ while 19% differentiated into Tbr2+ cells and 14% into Ctip2+ cells (Figure 3B–D, I). Overexpression of Tuba8 significantly increased the fraction of electroporated cells co-stained with Ctip2 (Figure 3B’–D’, E), indicating that Tuba8 electroporated cells commit to neurogenesis earlier than their control counterparts. In contrast, knockdown and knockout of Tuba8 increased the number of electroporated cells committed to the Tbr2+ cell fate (Figure 3B”–D”’, E). We concluded that Tuba8 induces a bias towards direct neurogenesis, an established characteristic of aIPs. The observed increase in the number of bIPs in Tuba8KO cortices was additionally confirmed at E12.5 and E13.5 (Figure S5G–J).

To gain more evidence that Tuba8 promotes direct neurogenesis, we measured single-pulsed BrdU levels in progeny of cells electroporated with Tuba8 expression or Tuba8 knockdown constructs (Figure 2F) (Cárdenas et al., 2018). Assuming that pCAG constructs require ~10 hours to deliver detectable levels of their RNA/protein products and that the E11.5 progenitor cell cycle lasts ~11.5 hours (Sahara, unpublished data), BrdU was injected 20 hours post electroporation, i.e. ~3 hours before the second mitosis. If cells stop proliferation and become neurons immediately, the BrdU intensity of their nuclei will be the highest (100%), while every additional round of cell division will dilute the BrdU signal twofold. Analysis of E14.5 sections when most of the GFP+ cells migrate to the CP showed that Tuba8 overexpression increased the fraction of high-BrdU labelled cells, while Tuba8 knockdown increased the fraction of lower-BrdU labelled cells (Figure 3G–J). This supports our data described above.

To visualize the fate of cell progenies upon manipulation of the Tuba8 levels, we traced the trajectories of dividing cells in slice culture (Figure 3K–N). Tuba8 overexpression increased the fraction of dividing cells generating neurons while its knockdown increased the

incidence of bIPs. Together, these data indicate that Tuba8 promotes the direct neurogenesis pathway.

Manipulation of progenitor fates by Tuba8 results in distinct lineage outcomes in the postnatal cortex

To directly test fate differences between RGs and aIPs, we analysed cortical neurogenesis outcomes following changes in Tuba8 levels (Figure 4A–L). We electroporated a Cre recombinase construct in the co-transfection mixture in ROSA26-tdTomato reporter (Ai9) embryos to monitor a bulk of neuronal lineages of electroporated progenitors (Madisen et al., 2012). In the somatosensory areas of P10 cortices electroporated with control vector, tdTomato+ cells were found in all layers but showed the highest densities in layer (L) 4 and 6 (Figure 4B–B”, E). Progenies of Tuba8-electroporated progenitors were distributed evenly across the all layers (Figure 4C–C” E). On the other hand, progenies of Tuba8 knocked down progenitors were unevenly distributed with a significant reduction of L5 neurons and an increase in the number of L2/3 and L6 neurons (Figure 4D–D”, E). In agreement with the Tuba8KD phenotype, Tuba8KO showed a reduction in the number of L5 neurons and the increase of L4 neurons. (Figure 4F–J’, K).

We further explored which neuronal subtypes were affected by Tuba8 manipulation by using the Satb2 marker for callosal projection neurons, Ctip2 for subcerebral projection neurons, and RORβ for L4 spiny neurons, respectively (Harb et al., 2016; Molyneaux et al., 2015). Interestingly, affected neuronal types were mostly Satb2+ and Ctip2+ single-positive cells in L5 and RORβ/Satb2+ cells in L4. Ctip2/Satb2 double-positive cells, which represent subclasses of L5 neurons, were unchanged (Figure 4E, K). These data are consistent with the recently published results on cortical progenitor diversity, where significant number of progenitor lineages showed a “L5-skipped” behaviour (Llorca et al., 2019). We conclude that the Tuba8-controlled transition between aRGs and aIPs culminates in distinct neuronal lineage outcomes.

Substitution of the C-terminal phenylalanine with tyrosine abolishes the ability of Tuba8 to promote the aIP fate, but is not sufficient to induce supernumerary RG fibers

The last amino acid residue of the Tuba8 chain is phenylalanine (F), which differentiates it from other Tuba isotypes containing a C-terminal tyrosine (Y) (Stanchi et al., 2000). We therefore wondered if this substitution plays a role in aIP fate induction. We generated two Tuba8 mutants, one with the C-terminal tail swapped with that of Tuba1a (which has a C-terminal Y; Tuba8-C-1a) and another where the C-terminal F was substituted with a Y (Tuba8F/Y) (Figure 5). We tested the effects of these proteins on the activation of pBlbp and pTα reporters (Figure 5A–E), as well as basal RG fiber formation (Figure 5F–J). As shown in Figure 6N, the use of the same CAG promoter should lead to comparable expression levels of different tubulins. Notably, both of these constructs failed to increase the proportion of pTα+ cells or to promote shortening of basal RG fibers (Figure 5E, J). This demonstrates the crucial role of the C-terminal F residue in the induction of aIP fate. However, introduction of these mutants failed to induce the supernumerary RG fibers observed in Tuba8 knockdowns or knockouts (Figure 2), suggesting that a secondary mechanism must be required for the induction of basal RG fibers.

Tuba8 C-terminal tail is immune to detyrosination and Δ2 cleavage

Besides the C-terminal F, Tuba8 has other unique features including the lack of a lysine (K) 40 residue, a target for acetylation in other tubulin isotypes, and a C-terminal amino acid sequence generally different from other Tuba family members (Figure 6A) (Stanchi et al., 2000). These structural features suggest that Tuba8 may have an effect on PTM patterns of MTs, which might in turn modulate aIP induction, as shown by the importance of K-acetylation in neuronal migration (Creppe et al., 2009). To test this possibility, we investigated tubulin PTMs in Tuba8KO and WT cortices with antibodies against major tubulin PTMs, including acetylation, poly-glutamination (polyE), detyrosination, tyrosination, and Δ2-tubulin (Figure 6B–J). To examine PTM levels in progenitors, we isolated them as Prominin-1+ cells using MACS sorting (Figure 6H). While the levels of acetylation, tyrosination and detyrosination remained relatively stable, we detected an increase in the Δ2-tubulin and poly-E signals (Figure 6I, J). In a complementary experiment where we overexpressed Tuba8, we found a robust decrease in Δ2-tubulin and detyrosnation levels, while the poly-E levels remained unchanged (Figure 6K–M). Since Δ2-tubulins are generated from detyrosinated tubulin in a reaction catalysed by the CCP enzyme family (Rogowski et al., 2010), this reduction in detyrosinated tubulins could be due to their irreversible conversion to Δ2-tubulin. These data suggest that Tuba8 supresses the level of Δ2-tubulin in the developing cortex.

To gain an insight into how Tuba8 supresses the levels of Δ2-tubulin, we examined the sensitivity of Tuba8 to tyrosination/detyrosination and Δ2 PTM in the presence of the Vash1/Svbp1 complex. Vash1/Svbp1 has been reported to induce tubulin detyrosination (Aillaud et al., 2017; Nieuwenhuis et al., 2017). Similar to the phenotype of tubulin tyrosine ligase mutant mice, we also found that the level of Δ2-tubulin increases upon the overexpression of Vash1/Svbp1 (Figure 6N), suggesting that detyrosination triggers the subsequent cleavage to Δ2-tubulin by endogenous CCPs. We used Venus-tagged constructs to distinguish overexpressed Tuba and endogenous tubulins In HEK293 cells. The constructs included Venus-tagged Tuba8, Tuba8F/Y, Tuba1a (the most abundant and well-characterized Tubulin-α found in the developing cortex (Braun et al., 2010)), and chimeric Tuba8 with a C-terminal tail of Tuba1a (Tuba8-C-1a). To our surprise, both Tuba8 and Tuba8F/Y maintained relatively high levels of tyrosine/phenylalanine modifications even in the presence of Vash1/Svbp1 (Figure 6N, O). Although both tubulins were detyrosinated by Vash1/Sbvp1 as shown previously (Nieuwenhuis et al., 2017), the Δ2 levels of Venus-Tuba8 and Venus-Tuba8F/Y were noticeably lower compared to Venus-Tuba1a. These results suggest that the C-terminal tail of Tuba8 is relatively resistant to detyrosination, which may in turn inhibit generation of the Δ2 forms (Figure 6P). Unexpectedly, the efficiency of Tuba8-C-1a detyrosination and Δ2 cleavage was relatively high, pointing at a possible role of an isotype-specific regulatory interaction between tubulin core and the C-terminus in determining the extent of C-terminal PTMs.

Δ2/3-tubulins induce supernumerary basal RG fibers and promotes indirect neurogenesis

The negative effect of Tuba8 on the Δ2-tubulin abundance suggested the possibility that this PTM may contribute to the over-production of RG fibers in Tuba8KO and knockdown cortices. To test this directly, we firstly created a dominant negative mutant of Tuba8 in

which two of its C-terminal amino acid residues were deleted (Tuba8Δ2). Strikingly, we observed a robust induction of RG fibers in Tuba8Δ2-electroporated brains (Figure 7B–B”’, F). The increased levels of Δ2-tubulin in Tuba8KO cortices appear to result from endogenous tubulin PTMs. It has been reported that CCP catalyses further cleavage into Δ3-tubulin, and that Δ2 and Δ3 forms co-exist in the developing brain (Aillaud et al., 2016). Although we were unable to measure the level of Δ3-tubulins in Tuba8KOs due to the lack of a commercially available antibody, we tested the effects of both Tuba1aΔ2 and Tuba1aΔ3 on RG fiber formation, assuming that Δ3-tubulin generation can be stimulated by the Vash1/Svbp1. Similar to Tuba8Δ2, we observed an induction of supernumerary RG fibers following the overexpression of Tuba1aΔ2 and Δ3 (Figure 7C–D”’, F).

Furthermore, we examined the role of the Vash1/Svbp1 complex, which facilitates Δ2 cleavage of endogenous tubulin (Figure 6N). Overexpression of Vash1/Svbp1 increased the number of basal RG fibers (Figure 7E–E”’, F). Interestingly, we noticed that co-electroporation of Tuba1aΔ3 or the Vash1/Svbp1 led to the development of large and elongated radial endfeet contacting the basal lamina (Figure 7D’–E”’), a similar phenotype to that of Tuba8KO and knockdown (Figure 2), or RG endfeet observable at E14.5 (Figure S3). In contrast, electroporation of Tuba8Δ2 and Tuba1aΔ2 produced thin, rod-like RG endfeet (Figure 7B–C”’). These morphological differences may reflect the accumulation of Δ3-tubulin over time, as Δ2/3-cleavage is an irreversible reaction (Aillaud et al., 2016; Paturle-Lafanechere et al., 1994). To confirm that Tuba8 C-terminal tail is responsible for shortening RG fibers, we tested Venus-Tuba8-C-1a, a protein no longer resistant to the Δ2 modification (Figure S6). Contrast to the effect of Tuba8, the swapping construct labelled the RG fibers (Figure S6A–C). Venus fluorescence was also observed in supernumerary RGs induced by Vash1/Sbp1 (Figure S6A’–C’). Taken together, these data suggest that Δ2/3-tubulins can help basal RG fibers maintain contact with the basal lamina. Tuba8 antagonizes this PTM, thus, promoting a transition of RG to the aIP fate (Figure 7G).

RG fibers are known to transduce integrin signalling from the basal membrane and maintain RG identity (Fietz et al., 2010; Long et al., 2016). We, therefore, sought to investigate whether integrin signaling was active in Δ2/3-tubulin induced RG fibers. We used the 9EG7 antibody that recognizes the conformational changes of integrin B1 observed upon integrin activation (Lenter et al., 1993). In controls, the 9EG7 signal was localized to the radial endfeet of RGs that were attached to the basal membrane (Figure S7A–D). In Vash1/Svbp1-overexpressing cortices, the endfeet of supernumerary RG fibers showed a similar 9EG7 staining pattern (Figure S7A’–D’), suggesting that Δ2-induced RG fibers sustain integrin signaling.

We have shown thus far that induction of Δ2/3-tubulin induces an excess of RG fibers that contact with the basal lamina and are receptive to integrin signalling. It is, however, apparent that they retain high pTα activity, a marker of aIP identity (Figure 7A–E”’, S7E-L). We therefore wondered whether these chimeric progenitors with basal RG fibers and high aIP promoter activity show a bias towards direct or indirect neurogenesis, one of prominent differences between RGs and aIPs (Figure 3; (Petros et al., 2015; Tyler and Haydar, 2013)). In order to address this question, we again measured the number of cells expressing Tbr2 and Ctip2 in cortices electroporated with the constructs facilitating Δ2/3-tubulin generation.

We found a greater fraction of Tbr2+ cells in cortices electroporated with constructs, which increase the levels of Δ2/3-tubulin (i.e. Tuba8Δ2, Tuba1Δ2, Tuba1aΔ3, or Vasp1/Svbp1), at the expense of Ctip2+ cells (Figure 7H–K). This data suggests a role of Δ2/3-tubulin in dictating the choice between direct or indirect neurogenesis, which could be mediated by signal(s) transmitted through contact with the basal lamina (Figure 7L, S7).

Discussion

Our data argue that tubulin PTMs play a critical role in differentiation of cortical progenitor cells. Indeed, the expression of an atypical tubulin isotype, Tuba8, at the onset of neurogenesis drives differentiation of RGs into aIPs by perturbing two tubulin PTMs, namely tyrosination and Δ2-tubulin cleavage. The F residue in the Tuba8 C-terminal tail is essential for aIP induction through the shortening of basal RG fibers, promoting pTα activity, and introducing a bias towards direct neurogenesis. The C-terminal tail of Tuba8 also functions to inhibit detyrosination and Δ2-tubulin generation, which is required for basal RG fiber integrity and indirect neurogenesis.

Insights into aIPs biogenesis and subtype diversity

aIPs are a recently identified type of apical cortical progenitors and progeny of RGs (Gal et al., 2006; Pilz et al., 2013). However, the mechanisms responsible for the fate switch from RGs to aIPs are unknown. In the vTel, time-lapse imaging demonstrates that aIPs are generated when one of the daughter cells does not inherit nor extend a new basal process after RG asymmetric divisions (Falk et al., 2017). Therefore, the shortened nature or absence of a basal process in aIPs is likely due to the inability of the aIPs to extend a fiber towards the basal lamina, rather than the degradation or truncation of an existing inherited RG fiber. In this study, we show that C-terminal tail of Tuba8 is essential to perturb two PTMs, tyrosination and cleavage of tubulins into Δ2-tubulin, which are crucial for the generation of basal RG fibers. Tuba8-positive cells are, therefore, more likely to adopt aIP fate. An important question for further studies is whether this process occurs in a deterministic or random manner in vivo. The expression of Tuba8 is restricted to a subset of progenitors. If this expression oscillates, as seen with Notch signaling (Shimojo et al., 2008), aIP fate may be defined in a random fashion. Conversely, if its expression is static, then aIP fate is likely determined early on when Tuba8 expression peaks. A fate mapping study by Cre recombination should allow us to distinguish between these possibilities.

In the developing cortex, we observed at least two types of aIPs at E12.5, one lacking basal fibers, and another with basal processes ending at the border between the VZ and CP (Figure 2). In the vTel where Tuba8 is also highly expressed (Figure 1), aIPs lack basal processes (Falk et al., 2017; Pilz et al., 2013). RG subtypes, which possess shorter RG fibers anchored to blood vessels (Tan et al., 2016), are reminiscent of cortical aIPs. In the developing human cortex, it has been shown that RGs transform into “truncated” forms in which their basal RG fibers terminate in the deep cortical walls (Nowakowski et al., 2016). Although the relationship among mouse blood vessel-anchored RGs, human truncated RGs, and cortical aIPs is not entirely clear, it would be intriguing to investigate the involvement of tubulin PTMs in the emergence of these distinct subtypes of intermediate progenitors.

Functional impacts of tyrosine and phenylalanine on tubulin PTMs during corticogenesis

Tubulin tyrosination has been studied in many biological contexts, including cell division, cell motility, and morphogenesis (Barisic and Maiato, 2016; Gadadhar et al., 2017; Nieuwenhuis and Brummelkamp, 2018). In mammals, Tuba8 is the only tubulin naturally terminating with an F residue (Stanchi et al., 2000), although F can be incorporated post-translationally (Ditamo et al., 2016). Phenylketonuria is a metabolic genetic disorder caused by the mutation of phenylalanine hydroxylase in which the levels of F in the blood are elevated, leading to mental retardation (Brown and Lichter-Konecki, 2016). In the phenylketonuria rat model, the levels of F-modified tubulin are 8-fold higher than in controls and those of tyrosinated tubulin are 8-fold lower (Rodriguez and Borisy, 1979). In mouse neuron-derived cell lines, the addition of F has been shown to inhibit neurite retraction and reduce MT dynamics at the growth cone (Ditamo et al., 2016). In our study of F/Y substitution, we demonstrate that F in the Tuba8 C-terminal tail is essential for the induction of aIPs with shorter RG fibers, indicating that an impact of F residue on tubulin C-terminal tail, possibly disturbing Y-mediated protein interaction to the MT regulators (Nirschl et al., 2016; Peris et al., 2006). If any of the MT regulatory proteins showed different binding affinities between F and Y, we would expect different MT behaviours and consequently different MT functions.

The function of Δ2/3-tubulin in corticogenesis

Δ2-tubulins are found in the long-lived MTs of differentiated neurons, the axonemes of cilia and flagella, and centrioles. They are, therefore, thought to contribute to MT stability (Paturle-Lafanechere et al., 1994). In the brain, approximately 35% of tubulins cannot be re-tyrosinated because they lack C-terminal second glutamic acid residues, an irreversible PTM (Paturle-Lafanechere et al., 1994). Δ2/Δ3-tubulin are generated from detyrosinated tubulin in a reaction catalyzed by the CCP family of enzymes (Aillaud et al., 2016), such that Δ2/Δ3-tubulin generation is indirectly regulated by the tyrosination/detyrosination cycle. In our study, we demonstrated that Δ2/3-tubulins promote the maintenance of RG fibers that contact the basal lamina. Overexpression of Δ2/3-tubulin in cortical progenitors creates a bias towards indirect neurogenic pathways, indicating that Δ2/3-tubulin affects the division modes of apical cortical progenitors.

How does Δ2/3-tubulin control progenitor fate? There are at least two possible, but not mutually exclusive, mechanistic explanations. One is that, as we observed, basal RG fibers induced by Δ2/3-tubulins maintain the proliferative potentials of RGs by conveying signals from basal lamina, including integrin signalling, and, thereby promoting the generation of bIPs. An alternative hypothesis is that the accumulation of Δ2/3-tubulins changes the cell division mode by either affecting the stability of astral/polar MTs and/or the centrosomes of mitotic cells. Given the importance of tyrosination/detyrosination of tubulin in mitosis (Barisic et al., 2015), and the biased orientation of centromeres in meiosis (Akera et al., 2017), although we did not see any effects of Tuba8 on the spindle orientation (Figure S4), an attractive idea would be to examine the possible asymmetry of tyrosination/detyrosination and Δ2-tubulin distribution in the mitotic spindles of cortical progenitors. Recently, three molecular mechanisms (hyperpolarization/WNT activity, unfolded protein response, and Robo/Dll1 signalling) have been suggested to balance direct vs. indirect neurogenesis in

mid-corticogenesis (Cárdenas et al., 2018; Laguesse et al., 2015; Vitali et al., 2018). Understanding the possible regulatory relationship between these signalling pathways and Δ2/3-tubulin-mediated effects in the early corticogenesis may be informative. It is also worth noting that Vash1 was recently identified as a target of FMRP at basal RG endfeet (Pilaz et al., 2016), which may function to stabilize RG endfeet locally by creating Δ2/3-tubulin.

Tubulin codes and tubulin isotypes in cell fate decision

Despite the high structural similarity among tubulin family members, the functions of specific isotypes have only just begun to be acknowledged (Breuss et al., 2017; Chakraborti et al. 2016; Romaniello et al., 2018). In our study, we present evidence that Tuba8 drives aIP differentiation from RGs, which is the first example of tubulin isotypes and their respective PTMs controlling cell fate decisions. Although Tuba8KO cortex shows no gross morphological phenotypes and the link between Tuba8 and polymicrogyria is currently debated (Diggle et al., 2017), we show that a change in the aIP and aRG abundance triggered by Tuba8 level manipulations alters the neuronal differentiation outcomes especially evident in the L4 and L5 populations. This argues that Tuba8 may modulate neuronal diversity within cortical layers. It will be interesting to see if the Tuba8-controlled aRG/aIP transition contributes to the emergence of recently identified heterogenous translaminar lineages including those skipping L4 or L5 (Llorca et al., 2019).

Contrary to the assumption that the functions of tubulin isotypes might be largely redundant, our work illustrates that the unique sequence of the Tuba8 C-terminal tail promotes biogenesis of aIPs accompanied by a loss of basal RG fibers. Since the C-termini of different tubulin isotypes vary in length and amino acid composition, further studies in this area will likely uncover new roles of this protein family in regulation of important developmental and physiological decisions. In light of our present work, it will be especially interesting to systematically evaluate possible roles of a tubulin C-terminal “code” in controlling morphology, division modes, response to external cues, and differentiation potential of neural progenitor cells.

STAR Methods

Lead Contact and Materials Availability

Further information and requests for resources and reagents should be directed to and will be fulfilled by the Lead Contact, Setsuko Sahara (setsuko.sahara@kcl.ac.uk).All unique/stable reagents generated in this study are available for request from the Lead Contact without restriction, although transfer of Fgf10 floxed mice will require a completed Materials Transfer Agreement.

Experimental Model and Subject Details

Mice

All experimental procedures are approved by the United Kingdom Home Office. The day of insemination and day of birth were designated E0.5 and P0, respectively. C57BL/6J, CD-1 and Tuba8$^{em1(IMPC)J}$ were housed and bred in the KCL animal facility Breeding and timed

mating of mice at the University of Minnesota are approved by the University of Minnesota IACUC. In both facilities, mice are maintained on 12h light:dark cycles at room temperature. Fgf10 floxed mice (Figure S1) were bred with CMV-Cre mice. The offspring was further bred with C57BL6/J mice to segregate the Cre transgene. Germline deletion of the floxed sequence to generate $Fgf10^{+/Flox\text{-}del}$ mice was confirmed by genomic PCR. The $Fgf10^{+/Flox\text{-}del}$ males and females were set for timed mating to collect E11.5 embryos. The Fgf10 $^{Flox\text{-}del/Flox\text{-}del}$ embryos were determined by the lack of limb buds. $Tuba8^{em1(IMPC)J}$ were genotyped using the primer set described in Table S3. Samples were harvested from males and females at the various developmental stages indicated in each figure legend (E9.5 to E15.5 and P10, and 16).

Cell Lines and Culture

HEK293 cell lines were cultured in DMEM (Thermo Fisher Scientific Cat# 61965026) supplemented with 10% Heat inactivated fetal bovine serum (Cat# 10082147), and were maintained at 37°C with 5% CO_2.

Methods Details

Generation of Fgf10floxed mice

Floxed Fgf10 mouse line was generated as previously described with some modifications (Sekine et al., 1999). The floxed Neo cassette was introduced into the EcoRI site located downstream of exon1. The additional LoxP sequence was inserted in the KpnI site upstream of exon1 to delete the first transcriptional starting site. The recombination to the correct loci was confirmed by PCR (Figure S1) with primers shown in Table S3.

Plasmids

All plasmids used in this study were purified by PureLink HiPure Plasmid Maxiprep Kit (Thermo Scientific) according to the manufacturer's protocol. pCAG-GFP and pCAG vectors have been described previously (Sahara and O'Leary, 2009). cDNAs inserted into pCAG vector were constructed as below. All oligonucleotide sequence information can be found in Table S3. The pBlbp reporter construct was a kind gift from Dr Heinz, in which we substituted the CAG promoter of a pCAG-GFP construct to generate pBlbp-GFP vector. The pTα-GFP construct was a kind gift from Dr Haydar (Gal et al., 2006). The CAG promoter of a pCAG-GFP construct was substituted using the SalI-BamHI site of the pTα-DsRed construct to create pTα-mCherry.

pCAG-Tuba8:

EcoRI-SalI fragment of Image clone 4507364 was subcloned. pCAG- pCAG-H2BtagBFP-Tuba8 miR-RNAi: two miR-RNAi were designed by BLOCK-iT RNAi Designer (Table S3), and subcloned in tandem into pcDNA6.2-GW/miR. For an efficient knockdown, we combined two miRNA domains into one plasmid b subcloned the HincII-Xho fragments into the SalI-XhoI site of pCAG-H2BtagBFP. pCAG-Tuba1a, pCAG-Vash1, pCAG-Sbvp1, pCAG-Tuba8F/Y, pCAG-Tuba8Δ2, pCAG-Tuba1aΔ2: cDNA fragments using primers described in Table S3 and E13.5 cortices cDNA or subcloned cDNA as a template were amplified by Q5 High-Fidelity DNA polymerase (New England Biolabs), and subcloned into

home-made TA vector based on pBluescript, followed by further subcloning into a pCAG vector (Sahara et al., 2007). pCAG-Tuba8-C-1a: Nested PCR using four primers were used to create a fusion construct. pCAG-Venus-Tuba8, pCAG-Venus-Tuba1a, pCAG-Venus-Tuba8F/Y: Venus cDNA (gifted from Dr Lim, O. Marin's lab) were PCR-amplified and subcloned into the EcoRI-EcoRV site of pCAG-Tuba8, pCAG-Tuba8F/Y, or of pCAG-Tuba1a. EcoRV-XhoI fragments of pCAG-stop-CD14-iresGFP (gifted by Dr Matt Grubb) were subcloned into pCAG vector to create pCAG-CD14-iresGFP.

In utero electroporation and in utero injection of Fgf10 protein

In utero electroporation of E11.5 or E13.5 embryos was performed as previously described with some modifications (Sahara et al., 2007). WT CD-1 or Tuba8KO mice were anesthetized using isoflurane. DNA solution (1 mg/ml of each construct + 0.05% Fast green in PBS) was injected into the lateral ventricles of embryos using pulled glass micropipettes. Five electric pulses (50 msec, 950 msec intervals) (Square Wave NEPA Gene Electroporator) at 27V (E11.5) or 32V (E13.5) were given by placing the embryo's head between triple platinum electrodes (2.0 mm diameter circle, tweezer electrodes for cathode) (Sonidel Limited, U.K.), and a 2.0mm square electrode made in house for anode (dal Maschio et al., 2012). Embryos were harvested at the stages indicated in each experiment.

In utero injection of Fgf10 protein at E10.5 was performed under the surgical conditions described above. 1 mg/ml of Fgf10 protein or PBS was injected into the lateral ventricles. Tissue was harvested 24 hours later for RNA seq analysis.

In situ hybridization, immunohistochemistry, and imaging

A unique region of Tuba8 with the minimum overlapping with other α/β tubulins (57– 290 bp of NM_017379.2) was PCR amplified and subcloned into pBluescript to generate digoxigenin-labelled riboprobes. Mouse embryos were fixed in 4% PFA for 2 hours followed by overnight cryoprotection in 23% sucrose in DEPC-PBS. 20 μm sections of embryonic brains were processed for *in situ* hybridization as described previously (Sahara and O'Leary, 2009), following Allen Brain Atlas protocols (http://help.brain-map.org/download/attachments/2818169/ABADataProductionProcesses.pdf) with some modifications, such as the use of tyramide-DIG signal amplification (Hopman et al., 1998) using the TSA Plus DNP system (Perkin Elmer). Visualization was achieved via a BCIP/NBT reaction using an alkaline phosphatase-conjugated DIG Fab antibody (Sigma).

RNA sequencing

Total RNA was prepared by using RNeasy Micro kit (Qiagen). Four biological replicates/groups were prepared, and 1 μg of total RNA was used for library synthesis. Sequencing was performed using the Illumina HiSeq 2500 system 50 bp paired end read using v4 chemistry. Sequence alignment and analysis was done as previously described (Yap et al., 2018). We analyzed Transcriptome comparing E11.5 Fgf10KO cortices to WT (Loss-of-function, LOF), and Fgf10 protein-injected cortices to mock injections (Gain-of-function, GOF). Genes downregulated >1.67-fold in Fgf10KO cortices and upregulated >1.67-fold in Fgf10-injected cortices compared to corresponding controls ($p<0.05$) were shortlisted for further analyses.

Quantitative RT-PCR

The total RNA of embryonic cortices was extracted using TRIzol reagent (Thermo Fisher Scientific), and subjected to cDNA synthesis according to the manufacturer's protocol (RevertAid First Strand DNA Synthesis Kit, Thermo Fisher Scientific). The cDNA was used for qPCR with Maxima SYBR Green/ROX master mix. Thermocycling was performed using the Roche LightCycler 480 Instrument II. qPCR primers used are listed in Table S3. In Figure 1C and S2K, data were normalized by GAPDH expression, followed by the value at the earliest embryonic stage of the assay and are represented as mean ± SEM.

Transfection of HEK293 cells and immunoblot analysis

Venus-tagged Tuba constructs were transfected into HEK293 cells in the presence or absence of Vash1/Svbp1 with Lipofectamine3000 (Thermo Fisher Scientific). according to the manufacturer's protocol. Cells were lysed after 24h in Laemmli buffer and subjected to SDS-PAGE with a 10% acrylamide gel, followed by transfer to a PVDF membrane (Millipore) and incubation with primary antibody overnight at 4°C. Signals were detected through incubation with fluorescent antibodies enabling the dual detection of tubulin PTMs and α-tubulin (internal control).

MACS sorting of cortical progenitors and electroporated cells

E13.5 cortices from the WT or Tuba8 embryos were dissected out and dissociated as described previously (Qian et al., 1998). Briefly, cortices were incubated with 5 units/ml papain (Sigma) and 1mM N-acetyl-cysteine (Sigma) in DMEM for 3 min at room temperature, rinsed three times with MACS buffer (0.5% BSA, 2mM EDTA in PBS), and dissociated in 1 ml of MACS buffer via pipetting with a polished Pasteur pipette 20 times. The cell suspension was filtered through 40 μm cell strainer (Greiner Bio One), and centrifuged 1,200 rpm for 5 min. Cell pellets (10^7 cells) were resuspended in 180 μl of MACS buffer with 10 μl of anti-CD133 (Prominin-1) magnetic beads (Miltenyi Biotec) and incubated for 15 min on ice. Cells were washed with MACS buffer and loaded into pre-washed MS columns (Miltenyi Biotec), followed by the three washes with 500 μl of MACS buffer. Magnetically sorted cells were flushed out with 1 ml of MACS buffer, centrifuged 1,200 rpm 10 min at 4°C. Sorted cell pellets were immediately incubated 3 min at 100°C in Laemmli buffer and subjected to immunoblotting analysis. For sorting the electroporated cells, a pCAG-CD14-iresGFP construct (Bryson et al., 2014) was co-electroporated to E12.5 embryonic cortices and dissected out cortical tissues with GFP signals for sorting. Dissociated electroporated cells were sorted as described above using anti-CD14 beads instead of anti-CD133.

Immunocytochemistry of brain sections

Embryonic (30 μm thickness) and postnatal brain sections (40 μm thickness) were prepared as previously described with the following modification (Sahara and O'Leary, 2009). Sections were incubated in Antigen Unmasking solution (Citric Acid based, Vector Lab) at 70°C for 3 hours, followed by a 1 hour incubation period with 4% BSA for blocking, primary antibody overnight at 4°C, washed three times for 10 min with T-TBS, and

secondary antibody for 2 hours at room temperature. After a further wash with T-TBS, sections were mounted in FluoroGold Mounting medium (Thermo Fisher Scientific).

BrdU dilution experiment

A single injection of Bromodeozyuridine (BrdU; 10 mg/ml BrdU in 0.9% NaCl (Sigma), 50mg/kg of body weight) was injected intraperitoneally 20 hours post-electroporation, which is approximately 3 hours before the 2nd mitotic division (M2 in Figure 3F). Postmitotic cells with the highest BrdU signal (100%) were either generated directly from apical progenitors at M2 or from bIPs following their 1st mitotic division (M1), while those with 50% BrdU signal intensity were assumed to be generated via indirect neurogenesis. E14.5 embryos were fixed in 4% PFA and subjected to the immunostaining analysis.

Live imaging experiments

E11.5 embryos were electroporated with a mixture of pCAG-loxPSTOPloxP-ZsGreen (1 μg/μl), pCAG-Cre (20 ng/μl), and either of control, Tuba8, or Tuba8miRNAi vector. 16 hours after electroporation, embryos brains were dissected out, and sectioned at 250 μm in cold HBSS. Slices were placed on filter membranes (Millipore) containing DMEM/F12 with 5% fetal calf serum, 5% house serum, N2, B27, PenStrep, 0.7g/L glucose and 0.3g/L of sodium bicarbonate. Images were taken by Zeiss LSM880 with Airyscan with a 10x lens in 5% CO_2/37°C using the confocal z-stack function (10 μm) in every 20 min for 24 hours.

Optical Clearing of brain sections for RG fiber tracing

Fixed embryonic brain sections (80-100 μm thickness) in 4% PFA for 2 hours were mounted on Superfrost slides and subjected to the optical clearing as previously described with the modification (Ke et al., 2013). Sections were permeabilized in 0.3% TritonX-100 in TBS for 30 min, followed by overnight incubation with Omnipaque350 diluted 1/3 in T-TBS. The clearing medium was changed to ½ dilution for 10 hours and 1x Omnipaque350 overnight. Sections were mounted in 1x Omnipaque350 prior to confocal imaging.

Image Acquisition

In situ hybridization images were acquired using a Zeiss Axioskop connected to a cooled monochrome CCD camera (Retiga EXi Blue) and Volocity acquisition software. Confocal images were taken with a Zeiss LSM800 and 880, using the confocal z-stack function (0.43 μm intervals), or Airy-scan function (Figure 3K–M, S7).

Quantification and Statistical analysis

Image Quantification

Zen CZI files were converted into 16- or 8-bit TIFF files for analysis in ImageJ. All error bars are represented as mean ± SEM.

RNAseq analysis (Figure 1B)

Statistical values of RPKM reads are calculated by DESeq packages to model biological variation (n = 4 for each sample) (Friedman and Maniatis, 2011).

RT-qPCR analysis (Figure 1C, S2)

Total RNA from three independent embryonic cortices at indicated ages were subjected to qPCR. Gene expression values were determined relative to Gapdh transcript levels. Error bars are represented as mean ± SEM of three replicates**.**

pBlbp-GFP/pTα-mCherry promoter analysis (Figure 2I, 5E, S7E–L)

Embryonic cortical sections electroporated with pBlbp-GFP, pTα-mCherry, and pCAG-H2BBFP were imaged as z-stacks (0.43 μm intervals, 10 slices). Z-projection was performed as sum of slices. pCAG-H2BBFP+ cells in the VZ were counted as electroporated cells. For quantification of pBlbp+, pTα+, and pBlbp/pTα+ cells in sections of electroporated cortices, imaging condition (i.e. gain, laser power and pinhole) was determined using control brains such that the signal intensity in each color channel was optimally distributed without saturation. The same imaging condition was used for all the sections. Location of cells were registered based on the nuclear expression of CAG-H2BBFP using Cell Counter plugin running on ImageJ. Errors due to overlapping cells were manually corrected. For signals of pBlbp and pTα reporters, those less than 10% of the maximal intensity were regarded as negative (i.e. not significant). When a cell showed significant signals of the both reporters, it was regarded as double-positive if the intensity of weaker signal reached at least 30% of the other. Otherwise, the cell was regarded as single-positive for the dominant reporter. The number of pBlbp+ cells in controls (n=446 cells, 6 brains): 148, Tuba8 (n=281 cells, 7 brains): 40, Tuba8 miR-RNAi (n=433, 8 brains); 139, Tuba8KO (n=407, 7 brains): 155, Tuba8-C-1a (n = 537, 8 brains): 187, Tuba8F/Y (n = 243, 5 brains): 90, Tuba8Δ2 (n=385, 7 brains): 35, Tuba1aΔ2 (n = 264, 7 brains):11, Tuba1aΔ3 (n = 393, 8 brains): 38, Vash1/Svbp1 (n = 272, 7 brains): 30. The number of pTα+ cells in controls:70, Tuba8:183, Tuba8 miR-RNAi :15, Tuba8KO: 18, Tuba8-C-1a: 86, Tuba8F/Y: 35, Tuba8Δ2: 232, Tuba1aΔ2: 155, Tuba1aΔ3: 212, Vash1/Svbp1: 130.The number of pBlbl/pTα+ cells in controls: 210, Tuba8:55, Tuba8 miR-RNAi :260, Tuba8KO: 230, Tuba8-C-1a: 222, Tuba8F/Y: 97, Tuba8Δ2: 82, Tuba1aΔ2: 53, Tuba1aΔ3: 98, Vash1/Svbp1: 51. A chi-square test was performed to determine significant differences.

Basal RG fiber analysis (Figure2N, S3H, 5J, 7F)

30-μm cortical sections electroporated with pBlbp-GFP, pTα-mCherry and pCAG-H2BBFP were imaged as z-stacks (0.43 μm intervals from the top to the bottom of the section). The VZ region (200 μm-wide) of each z-stack image was cropped and used to count the number of electroporated cells labelled by pCAG-H2BBFP with 3D cell counter plugin (Fiji: above 30 voxels, 13000 threshold). The number of RG fibers was counted using background subtracted maximum projection images of the CP region (200 μm-wide) (background subtraction: Rolling ball radius, 50 pixels, threshold 0.8 pixels) and an Image J program that we created (fiber_profiler2.ijm in Data S1). Counts resulting from background noise were manually corrected. RG fibers were normalized by the number of cell bodies detected with the 3D cell counter plugin. The number of RG fibers / 100 electroporated VZ cells in controls (n= 6): 7.2 ± 0.70, Tuba8 (n = 5): 0.8 ± 0.38, Tuba8 miR-RNAi (n =6): 16.0 ± 1.25, Tuba8KO (n=7): 14.9 ± 1.52, Tuba8-C-1a (n =6): 8.4 ± 1.10, Tuba8F/Y (n 6): 7.5 ± 1.25, Tuba8Δ2 (n= 9): 16.0 ± 1.87, Tuba1aΔ2 (n = 5):21.8 ± 3.95 , Tuba1aΔ3 (n= 9) 18.6 ± 1.31,

Vash1/Svbp1 (n = 6): 15.3 ± 1.78. A One-way ANOVA with Dunnett's multiple comparisons test was used. In Figure 2J"'–M"', the intensity of red channel is increased for the better visualization of the RG fibers. Control and Tuba8 overexpression data from Figure 2 are included in Figure 5 and 7 for comparison between Tuba8 and Tuba8 mutant constructs.

Analysis of basal RG fiber stained by RC2 (Figure S3N)

20-μm E14.5 cortical sections stained with RC2 antibody were imaged as z-stacks (0.43 μm intervals from the top to the bottom of the section). Fibers were counted in 200 μm-wide sections of the CP, using fiber_profiler2.ijm. The number of RG fibers in the WT (n = 5): 38.8 ± 2.13, Tuba8KO (n = 5): 58.8 ± 2.96. An unpaired student's t-test was used.

pCAG-GFP basal RG fiber tracing analysis (Figure2T)

100-μm sections electroporated with pCAG-GFP and indicated plasmids were optically cleared by the SeeDB protocol and imaged as z-stacks (0.43 μm intervals, from the top to the bottom of the section). GFP+ fibers attached to the apical lamina were traced using NeuroTracer (Fiji). Fibers attached to the basal lamina were counted as "long" and those that terminated either within the VZ or CP were judged as "short". Progenitors cut at the edge of the imaged areas were excluded from the analysis. The number of long RG fibers in controls (n= 76, 3 brains): 46, Tuba8 (n = 61, 3 brains): 12, Tuba8 miR-RNAi (n=69): 52, Tuba8KO (n=75): 66, the number of short fibers in controls: 30, Tuba8: 49, miR-RNAi : 17, Tuba8KO: 9. A chi-square test was performed.

Tbr2/Ctp2 co-staining analysis in electroporated cortices (Figure3E, 7K, Figure S5G–J)

30-μm E12.5 electroporated cortical sections were stained using antibodies against tagRFP (for H2BBFP), Tbr2, and Ctip2, and imaged as z-stacks (0.43 μm intervals, 10 slices). In Figure S4, the antibody against tagRFP was omitted and counterstained by Dapi. Z-projection images created using the sum of slices were used for counting. The percentage of VZ cells that were Tbr2-/Ctip2- in the electroporated control: 63.5 ± 2.56, Tuba8: 50.5 ± 4.12, Tuba8 miR-RNAi : 57.4 ± 3.75, Tuba8KO:54.0 ± 0.02, Tuba8Δ2: 49.3 ± 0.00, Tuba1aΔ2: 50.8 ± 0.00, Tuba1aΔ3: 52.08 ± 0.00, Vash1/Svbp1: 56.9 ± 0.06, those of Tbr2+ cells in the electroporated control: 20.7 ± 2.27, Tuba8: 19.8 ± 0.77, Tuba8 miR-RNAi : 33.5 ± 0.01, Tuba8KO: 36.7 ± 2.38, Tuba8Δ2: 42.0 ± 1.40, Tuba1aΔ2: 41.4 ± 1.46, Tuba1aΔ3: 40.5 ± 2.90, Vash1/Svbp1: 39.0 ± 2.83, those of Ctip2+ in the electroporated control:15.8 ± 1.53, Tuba8: 29.7 ± 4.29, Tuba8 miR-RNAi : 9.11 ± 0.94, Tuba8KO: 9.28 ± 1.28, Tuba8Δ2: 8.67 ± 1.93 Tuba1aΔ2: 7.83 ± 0.50, Tuba1aΔ3: 7.41 ± 1.50, Vash1/Svbp1: 4.14 ± 0.94. The percentage of Tbr2+ cells in E11.5 WT under 200 μm column: 28.2 ± 4.00, E12.5 WT: 66.2 ± 4.60, E13.5 WT: 108 ± 8.30, E11.5 Tuba8KO: 30.3 ± 3.14, E12.5 Tuba8KO: 103 ± 7.06, E13.5 Tuba8KO: 188 ± 8.18. the percentage of Ctip2+ cells in E11.5 WT: 20.2 ± 2.90, E12.5 WT: 58.8 ± 5.04, E13.5 WT: 196.8 ± 7.61, E11.5 Tuba8KO: 67.4 ± 1.72, E12.5 Tuba8KO: 83.8 ± 7.25, E13.5 Tuba8KO: 177.6 ± 10.72. One-way ANOVA with Dunnett's multiple comparisons were used for Figures 3E and 7K, and a Two-way ANOVA with Sidak's multiple comparison test was used for Figure S6J.

Spindle orientation analysis of mitotic cells in anaphase (Figure S4)

30-μm E12.5 cortical sections from WT and Tuba8KO embryos were stained by the antibodies against γ-tubulin and Arl13b, and Dapi for nuclear staining, and imaged as z-stacks (0.43 μm intervals, 30 slices). Two centrosome positions stained by γ-tubulin, and five positions randomly selected at the apical membrane are used to determine the angles of mitotic spindles by using R script of Jüschke et al (Jüschke et al., 2014). The number of cells with an angle of 0-15° in controls (n= 36, 6 brains): 26, Tuba8KO (n = 49, 8 brains): 33 , those of 15-30° in controls: 9, Tuba8KO: 14, those of 30-45° in controls: 0, Tuba8KO: 2, those of 45-60° in controls: 1, Tuba8KO: 0. A chi-square test was performed.

Ctip2 co-staining analysis with PH3, Ki67 or Tbr1 (FigureS5A–F")

30-μm E12.5 WT cortical sections were stained by the antibodies against Ctip2 together with PH3, Ki67 or Tbr1, counterstained with Dapi, and (0.43 μm intervals, 5 slices). The fraction of Ctip2+/PH3+ cells in total PH3+ cells was 100.0 ± 0.00 (n = 6), that of Ctip2+/Ki67+ cells in total Ki67+ cells was 2.4 ± 0.60 (n = 4), and that of Tbr1+/Ctip2+ cells in total Ctip2+ cells was 67.6 ± 5.7 (n = 4). No Tbr1+/Ctip2- cells were detected.

Quantification of dividing cells in time-lapse imaging (Figure 3N)

Living slices electroporated with the control (n = 5 brains), Tuba8 (n = 7 brains), or Tuba8 miR-RNAi (n = 6 brains) vector were imaged as z-stacks (10 μm intervals, 10 slices). Acquired images were processed by Airyscan. Average or maximum projection images were used to monitor the behaviors of cells from each apical mitotic cell to determine the cell type of the progenies. The number of RG-RG divisions in controls (n= 29, 7 embryos): 17, Tuba8 (n = 26, 7 embryos): 9, Tuba8 miR-RNAi (n=24, 6 embryos): 13, the number of RG-bIP divisions in controls: 5, Tuba8: 2, miR-RNAi : 10, and the number of RG-N divisions in in controls: 7, Tuba8: 15, Tuba8 miR-RNAi : 1. A chi-square test was performed. We defined cells which underwent the second mitosis at the apical surface as RG (Video S1–3), those with a multipolar morphology that migrate towards and settle in the CP as neurons (Movie S2), and those undergoing mitosis either in the middle of the VZ or the CP , which generate progenies that migrate towards and settle in the CP as bIPs (Movie S3).

Immunostaining analysis of postnatal cortical sections (Figure 4E, K)

The primary somatosensory areas of immunostained P10 postnatal sections (40 μm) electroporated at E11.5 were imaged, and tdTomato+ cells under the 500 μm columns were counted. The cell number was normalized by the total tdTomato+ cells which excluded those with glial morphology with a smaller cell body and rich arborization processes. The percentage of total neurons in each cortical layer in the electroporated control (n =6 brains) : 27.5 ± 1.80 (L2/3), 22.1 ± 0.61 (L4), 18.8 ± 1.06 (L5), 31.60 ± 1.61 (L6), Tuba8 (n = 6 brains): 35.6 ± 1.92 (L2/3), 16.5 ± 1.04 (L4), 21.00 ± 1.50 (L5), 26.9 ± 2.0 (L6), Tuba8 miR-RNAi (n = 5 brains): 23.9 ± 0.45 (L2/3), 30.1 ± 1.81 (L4), 10.6 ± 1.12 (L5), 35.4 ± 1.85 (L6), Satb2+ neurons in the electroporated control: 26.6 ± 1.62 (L2/3), 20.6 ± 0.81 (L4), 11.1 ± 1.05 (L5), 13.2 ± 1.41 (L6), Tuba8: 33.16 ± 2.13 (L2/3), 15.1 ± 1.05 (L4), 13.5 ± 1.44 (L5), 9.07 ± 1.35 (L6), Tuba8 miR-RNAi: 24.7 ± 1.30 (L2/3), 27.4 ± 2.4 (L4), 6.20 ± 1.06 (L5), 16.1 ± 1.21 (L6), Ctip2+ neurons in the electroporated control: 0.33 ± 0.19

(L2/3), 0.079 ± 0.079 (L4),2.89 ± 0.54 (L5), 9.44 ± 1.04 (L6), Tuba8: 0.00 (L2/3), 0.36 ± 0.25 (L4), 3.50 ± 0.70 (L5), 8.65 ± 2.09 (L6), Tuba8 miR-RNAi: 0.26 ± 0.26 (L2/3), 0.00 (L4), 1.56 ± 0.20 (L5), 7.95 ± 1.60 (L6), Ctip2+/Satb2+ neurons in the electroporated control: 0.00 (L2/3), 0.23 ± 0.23 (L4), 3.83 ± 0.56 (L5). 7.23 ± 1.01 (L6), Tuba8: 0.87 ± 0.61 (L2/3), 0.095 ± 0.085 (L4), 2.74 ± 0.58 (L5), 6.91 ± 1.46 (L6), Tuba8 miR-RNAi: 0.00 (L2/3), 0.25 ± 0.25 (L4), 2.53 ± 0.85 (L5), 8.84 ± 0.47 (L6). Two-way ANOVA with Sidak's multiple comparison test was used.

Immunostained P16 cortical sections from WT and Tuba8KO postnatal brains with antibodies against Satb2/RORβ/Ctip2 were imaged, stained cells in the somatosensory areas under the 500 μm columns were counted. The percentage of total neurons in each cortical layer in the WT (n = 7 brains): 218.3 ± 11.7 (L2/3), 239.1 ± 8.31 (L4), 216.7 ± 7.00 (L5), 382.9 ± 14.00 (L6), Tuba8KO (n = 8 brains): 198.7 ± 5.41 (L2/3), 324.6 ± 9.42 (L4), 135.0 ± 3.77 (L5), 385.6 ± 7.74 (L6), Satb2+ neurons in the WT: 195.6 ± 10.4 (L2/3), 117.6 ± 12.2 (L4), 104.7 ± 5.48 (L5), 67.42 ± 9.67 (L6), Tuba8KO: 180.6 ± 5.58 (L2/3), 149.0 ± 10.7 (L4), 55.13 ± 2.35 (L5), 72.3 ± 6.67 (L6), RORβ+/Satb2 neurons in the WT: 3.28 ± 1.32 (L2/3), 105.9 ± 11.4 (L4), 6.29 ± 2.13 (L5), 0.00 (L6), Tuba8KO: 4.62 ± 0.96 (L2/3), 153.1 ± 6.56 (L4), 3.00 ± 0.22 (L5), 0.00 (L6), Ctip2+ neurons in the WT: 17.3 ± 1.66 (L2/3), 12.3 ± 0.60 (L4), 78.0 ± 3.45 (L5), 208.9 ± 6.71 (L6), Tuba8KO: 11.88 ± 1.27(L2/3), 15.6 ± 1.82 (L4), 53.9 ± 3.07 (L5), 225.88 ± 7.07 (L6), Ctip2+/Satb2+ neurons in the WT: 1.00 ± 0.38 (L2/3), 0.71 ± 0.16 (L4), 27.4 ± 2.33 (L5), 106.1 ± 3.78 (L6), Tuba8KO: 0.88 ± 0.49 (L2/3), 1.63 ± 1.00 (L4), 23.6 ± 2.82 (L5), 86.88 ± 7.43 (L6). Two-way ANOVA with Sidak's multiple comparison test was used.

Quantification of immunoblotting intensity of MACS sorted cell lysates and HEK293 transfected cell lysates (Figure 6J, M, O)

Fluorescence intensity of each band was measured using the LI-COR Image Studio software and background subtraction was performed using the median measured by selecting the top and bottom of the bands.

The intensity in Tuba8KO progenitors sorted by Prominin-1 (n = 4) was normalized to the pan-tubulinα signal, followed by the mean value of the WT progenitors (n = 4). Poly-E staining in the WT: 1.0 ± 0.06, Tuba8KO: 1.73 ± 0.18, Acetylated Tubulin in the WT: 1.0 ± 0.22, Tuba8KO: 0.89 ± 0.02, deY-tubulin in the WT: 1.0 ± 0.09, Tuba8KO: 1.03 ± 0.05, Y-tubulin in the WT: 1.0 ± 0.10, Tuba8KO: 1.18 ± 0.23, Δ2-tubulin in the WT: 1.00 ± 0.02, Tuba8KO: 1.26 ± 0.05.

The intensity in Tuba8-electroporated cortical cells (n = 4) was normalized to the pan-tubulinα signal, followed by the mean value of the control-vector electroporated samples (n = 4). Poly-E staining in the control: 1.00 ± 0.16, Tuba8: 0.80 ± 0.07, Acetylated Tubulin in the control: 1.00 ± 0.18, Tuba8: 0.72 ± 0.06, deY-tubulin in the control: 1.0 ± 0.19, Tuba8: 0.13 ± 0.03, Y-tubulin in the control: 1.0 ± 0.17, Tuba8: 0.87 ± 0.08, Δ2-tubulin in the control: 1.0 ± 0.26, Tuba8: 0.18 ± 0.017.

The intensity in co-transfected cells with Venus-tubulins together with Vash1/Svbp1 (n = 3) was normalized to the pan-tubulinα signal of Venus-fusion tubulins, followed by the mean

value of the intensity in Tuba1a transfected cells. Y-tubulin in Tuba1a: 1.0 ± 0.65, Tuba8: 159 ± 15.6 , Tuba8F/Y: 214 ± 43.0, Tuba8-C-1a 7.62 ± 3.45, deY-tubulin in Tuba1a: 1.0 ± 0.19, Tuba8: 0.56 ± 0.09, Tuba8F/Y: 0.85 ± 0.19, Tuba8-C-1a: 2.44 ± 0.27,Δ2-tubulin in Tuba1a: 1.0 ± 0.24, Tuba8: 0.19 ± 0.01, Tuba8F/Y 0.16 ± 0.08, Tuba8-C-1a: 80.6 ± 2.94. Student's t-test with BH correction were used.

Quantification of immunostaining intensity in WT and Tuba8KO cortices (Figure S2)

Immunostained cortical sections from WT and Tuba8KO embryos culled at the indicated stages were imaged as z-stacks (0.43 μm intervals, 5 slices). The average pixel intensity of z-projection images generated from the sum of slices (200 μm-wide) was quantified. The intensity was then normalized by the Nestin signal (Figure S2). The relative intensity in Tuba8KO cortices was calculated using WT values as the control. Glast in the E11.5 WT: 1.0 ± 0.02, Tuba8KO: 0.98 ± 0.08. Student's t-test with BH correction were used for Figures 5 and S2.

DATA AND CODE AVAILABILITY

The published article includes all datasets generated during this study. RNA-seq data were deposited in the ArrayExpress archive (accession: E-MTAB-8279). The imageJ macro used for RG fiber counting is attached as Data S1.

Supplementary Material

Refer to Web version on PubMed Central for supplementary material.

ACKNOWLEDGEMENTS

We thank Drs B. Berninger, J. Clarke, C. Houart, and O. Marín for their valuable comments on the manuscript, Drs S. Kato for Fgf10 floxed mice, N. Heintz and T. Haydar for plasmids, and Ms A. Arcourt for technical assistance. We are grateful to Dr L. Cancedda for advice on triple electrode setup, and Drs V. Borrell and L. Lim for valuable advice on revision experiments. This work was supported by the Biotechnology and Biological Sciences Research Council (grants BB/L00562X/1 to S.S. and BB/M007103/1 and BB/R001049/1 to E.V.M.), the Brain & Behaviour Research Foundation (Young Investigator Grant 20881 to S.S.), European Commission (H2020-MSCA-RISE-2016; Project ID 734791; E.V.M.), and the National Institute of Arthritis, Musculoskeletal and Skin Diseases of the National Institutes of Health, USA (R01AR064195; Y.K.). S.I.R. was supported by a LIDo studentship from the BBSRC.

Reference

Abdollahi MR, Morrison E, Sirey T, Molnar Z, Hayward BE, Carr IM, Springell K, Woods CG, Ahmed M, Hattingh L, et al. (2009). Mutation of the Variant α-Tubulin TUBA8 Results in Polymicrogyria with Optic Nerve Hypoplasia. Am. J. Hum. Genet. 85, 737–744. [PubMed: 19896110]

Aillaud C, Bosc C, Saoudi Y, Denarier E, Peris L, Sago L, Taulet N, Cieren A, Tort O, Magiera MM, et al. (2016). Evidence for new C-terminally truncated variants of α- and β-tubulins. Mol. Biol. Cell 27, 640–653. [PubMed: 26739754]

Aillaud C, Bosc C, Peris L, Bosson A, Heemeryck P, Dijk JV, Friec JL, Boulan B, Vossier F, Sanman LE, et al. (2017). Vasohibins/SVBP are tubulin carboxypeptidases (TCPs) that regulate neuron differentiation. Science 358, 1448–1453. [PubMed: 29146868]

Akera T, Chmátal L, Trimm E, Yang K, Aonbangkhen C, Chenoweth DM, Janke C, Schultz RM, and Lampson MA (2017). Spindle asymmetry drives non-Mendelian chromosome segregation. Science 358, 668–672. [PubMed: 29097549]

Anthony TE, Klein C, Fishell G, and Heintz N (2004). Radial glia serve as neuronal progenitors in all regions of the central nervous system. Neuron 41, 881–890. [PubMed: 15046721]

Arai Y, and Taverna E (2017). Neural Progenitor Cell Polarity and Cortical Development. Front. Cell. Neurosci. 11. [PubMed: 28217083]

Arlotta P, Molyneaux BJ, Chen J, Inoue J, Kominami R, and Macklis JD (2005). Neuronal subtype-specific genes that control corticospinal motor neuron development in vivo. Neuron 45, 207–221. [PubMed: 15664173]

Barisic M, and Maiato H (2016). The Tubulin Code: A Navigation System for Chromosomes during Mitosis. Trends Cell Biol. 26, 766–775. [PubMed: 27344407]

Barisic M, Sousa R.S. e, Tripathy SK, Magiera MM, Zaytsev AV, Pereira AL, Janke C, Grishchuk EL, and Maiato H (2015). Microtubule detyrosination guides chromosomes during mitosis. Science 348, 799–803. [PubMed: 25908662]

Belvindrah R, Natarajan K, Shabajee P, Bruel-Jungerman E, Bernard J, Goutierre M, Moutkine I, Jaglin XH, Savariradjane M, Irinopoulou T, et al. (2017). Mutation of the α-tubulin Tuba1a leads to straighter microtubules and perturbs neuronal migration. J Cell Biol 216, 2443–2461. [PubMed: 28687665]

Bertet C, Li X, Erclik T, Cavey M, Wells B, and Desplan C (2014). Temporal Patterning of Neuroblasts Controls Notch-Mediated Cell Survival through Regulation of Hid or Reaper. Cell 158, 1173–1186. [PubMed: 25171415]

Braun A, Breuss M, Salzer MC, Flint J, Cowan NJ, and Keays DA (2010). Tuba8 Is Expressed at Low Levels in the Developing Mouse and Human Brain. Am. J. Hum. Genet. 86, 819–822. [PubMed: 20466094]

Breuss MW, Leca I, Gstrein T, Hansen AH, and Keays DA (2017). Tubulins and brain development – The origins of functional specification. Mol. Cell. Neurosci. 84, 58–67. [PubMed: 28347630]

Brown CS, and Lichter-Konecki U (2016). Phenylketonuria (PKU): A problem solved? Mol. Genet. Metab. Rep. 6, 8–12. [PubMed: 27014571]

Bryson JB, Machado CB, Crossley M, Stevenson D, Bros-Facer V, Burrone J, Greensmith L, and Lieberam I (2014). Optical Control of Muscle Function by Transplantation of Stem Cell–Derived Motor Neurons in Mice. Science 344, 94–97. [PubMed: 24700859]

Cárdenas A, Villalba A, de Juan Romero C, Picó E, Kyrousi C, Tzika AC, Tessier-Lavigne M, Ma L, Drukker M, Cappello S, et al. (2018). Evolution of Cortical Neurogenesis in Amniotes Controlled by Robo Signaling Levels. Cell 174, 590–606.e21. [PubMed: 29961574]

Caron JM, Jones AL, and Kirschner MW (1985). Autoregulation of tubulin synthesis in hepatocytes and fibroblasts. J. Cell Biol. 101, 1763–1772. [PubMed: 3902854]

Chakraborti S, Natarajan K, Curiel J, Janke C, and Liu J The emerging role of the tubulin code: From the tubulin molecule to neuronal function and disease. Cytoskeleton 73, 521–550.

Chen B, Wang SS, Hattox AM, Rayburn H, Nelson SB, and McConnell SK (2008). The Fezf2–Ctip2 genetic pathway regulates the fate choice of subcortical projection neurons in the developing cerebral cortex. Proc. Natl. Acad. Sci. 105, 11382–11387. [PubMed: 18678899]

Creppe C, Malinouskaya L, Volvert M-L, Gillard M, Close P, Malaise O, Laguesse S, Cornez I, Rahmouni S, Ormenese S, et al. (2009). Elongator Controls the Migration and Differentiation of Cortical Neurons through Acetylation of α-Tubulin. Cell 136, 551–564. [PubMed: 19185337]

Diggle CP, Martinez-Garay I, Molnar Z, Brinkworth MH, White E, Fowler E, Hughes R, Hayward BE, Carr IM, Watson CM, et al. (2017). A tubulin alpha 8 mouse knockout model indicates a likely role in spermatogenesis but not in brain development. PLOS ONE 12, e0174264. [PubMed: 28388629]

Ditamo Y, Dentesano YM, Purro SA, Arce CA, and Bisig CG (2016). Post-Translational Incorporation of L-Phenylalanine into the C-Terminus of α-Tubulin as a Possible Cause of Neuronal Dysfunction. Sci. Rep. 6, 38140. [PubMed: 27905536]

Englund C, Fink A, Lau C, Pham D, Daza RA, Bulfone A, Kowalczyk T, and Hevner RF (2005). Pax6, Tbr2, and Tbr1 are expressed sequentially by radial glia, intermediate progenitor cells, and postmitotic neurons in developing neocortex. J Neurosci 25, 247–251. [PubMed: 15634788]

Erck C, Peris L, Andrieux A, Meissirel C, Gruber AD, Vernet M, Schweitzer A, Saoudi Y, Pointu H, Bosc C, et al. (2005). A vital role of tubulin-tyrosine-ligase for neuronal organization. Proc. Natl. Acad. Sci. 102, 7853–7858. [PubMed: 15899979]

Falk S, Bugeon S, Ninkovic J, Pilz G-A, Postiglione MP, Cremer H, Knoblich JA, and Götz M (2017). Time-Specific Effects of Spindle Positioning on Embryonic Progenitor Pool Composition and Adult Neural Stem Cell Seeding. Neuron 93, 777–791.e3. [PubMed: 28231465]

Fietz SA, Kelava I, Vogt J, Wilsch-Bräuninger M, Stenzel D, Fish JL, Corbeil D, Riehn A, Distler W, Nitsch R, et al. (2010a). OSVZ progenitors of human and ferret neocortex are epithelial-like and expand by integrin signaling. Nat. Neurosci. 13, 690–699. [PubMed: 20436478]

Fietz SA, Kelava I, Vogt J, Wilsch-Bräuninger M, Stenzel D, Fish JL, Corbeil D, Riehn A, Distler W, Nitsch R, et al. (2010b). OSVZ progenitors of human and ferret neocortex are epithelial-like and expand by integrin signaling. Nat. Neurosci. 13, 690–699. [PubMed: 20436478]

Friedman BA, and Maniatis T (2011). ExpressionPlot: a web-based framework for analysis of RNA-Seq and microarray gene expression data. Genome Biol. 12, R69. [PubMed: 21797991]

Gadadhar S, Bodakuntla S, Natarajan K, and Janke C (2017). The tubulin code at a glance. J Cell Sci 130, 1347–1353. [PubMed: 28325758]

Gal JS, Morozov YM, Ayoub AE, Chatterjee M, Rakic P, and Haydar TF (2006). Molecular and morphological heterogeneity of neural precursors in the mouse neocortical proliferative zones. J Neurosci 26, 1045–1056. [PubMed: 16421324]

Gao P, Postiglione MP, Krieger TG, Hernandez L, Wang C, Han Z, Streicher C, Papusheva E, Insolera R, Chugh K, et al. (2014). Deterministic Progenitor Behavior and Unitary Production of Neurons in the Neocortex. Cell 159, 775–788. [PubMed: 25417155]

Greig LC, Woodworth MB, Galazo MJ, Padmanabhan H, and Macklis JD (2013). Molecular logic of neocortical projection neuron specification, development and diversity. Nat. Rev. Neurosci. 14, 755–769. [PubMed: 24105342]

Hansen DV, Lui JH, Parker PRL, and Kriegstein AR (2010). Neurogenic radial glia in the outer subventricular zone of human neocortex. Nature 464, 554–561. [PubMed: 20154730]

Harb K, Magrinelli E, Nicolas CS, Lukianets N, Frangeul L, Pietri M, Sun T, Sandoz G, Grammont F, Jabaudon D, et al. (2016). Area-specific development of distinct projection neuron subclasses is regulated by postnatal epigenetic modifications. ELife 5, e09531. [PubMed: 26814051]

Hopman AHN, Ramaekers FCS, and Speel EJM (1998). Rapid Synthesis of Biotin-, Digoxigenin-, Trinitrophenyl-, and Fluorochrome-labeled Tyramides and Their Application for In Situ Hybridization Using CARD Amplification. J. Histochem. Cytochem. 46, 771–777. [PubMed: 9603790]

Hoyle HD, Turner FR, and Raff EC (2000). A Transient Specialization of the Microtubule Cytoskeleton Is Required for Differentiation of the Drosophila Visual System. Dev. Biol. 221, 375–389. [PubMed: 10790333]

Jüschke C, Xie Y, Postiglione MP, and Knoblich JA (2014). Analysis and modeling of mitotic spindle orientations in three dimensions. Proc. Natl. Acad. Sci. 111, 1014–1019. [PubMed: 24381158]

Ke M-T, Fujimoto S, and Imai T (2013). SeeDB: a simple and morphology-preserving optical clearing agent for neuronal circuit reconstruction. Nat. Neurosci. 16, 1154–1161. [PubMed: 23792946]

Kelly SM, Raudales R, He M, Lee JH, Kim Y, Gibb LG, Wu P, Matho K, Osten P, Graybiel AM, et al. (2018). Radial Glial Lineage Progression and Differential Intermediate Progenitor Amplification Underlie Striatal Compartments and Circuit Organization. Neuron 99, 345–361.e4. [PubMed: 30017396]

Kosodo Y, Suetsugu T, Suda M, Mimori-Kiyosue Y, Toida K, Baba SA, Kimura A, and Matsuzaki F (2011). Regulation of interkinetic nuclear migration by cell cycle-coupled active and passive mechanisms in the developing brain. EMBO J. 30, 1690–1704. [PubMed: 21441895]

Laguesse S, Creppe C, Nedialkova DD, Prévot P-P, Borgs L, Huysseune S, Franco B, Duysens G, Krusy N, Lee G, et al. (2015). A Dynamic Unfolded Protein Response Contributes to the Control of Cortical Neurogenesis. Dev. Cell 35, 553–567. [PubMed: 26651292]

Lecine P, Italiano JE, Kim S-W, Villeval J-L, and Shivdasani RA (2000). Hematopoietic-specific β1 tubulin participates in a pathway of platelet biogenesis dependent on the transcription factor NF-E2. Blood 96, 1366–1373. [PubMed: 10942379]

Lenter M, Uhlig H, Hamann A, Jenö P, Imhof B, and Vestweber D (1993). A monoclonal antibody against an activation epitope on mouse integrin chain beta 1 blocks adhesion of lymphocytes to the endothelial integrin alpha 6 beta 1. Proc. Natl. Acad. Sci. 90, 9051–9055. [PubMed: 7692444]

Llorca A, Ciceri G, Beattie R, Wong FK, Diana G, Serafeimidou-Pouliou E, Fernández-Otero M, Streicher C, Arnold SJ, Meyer M, et al. (2019). A stochastic framework of neurogenesis underlies the assembly of neocortical cytoarchitecture. ELife 8, e51381. [PubMed: 31736464]

Long K, Moss L, Laursen L, Boulter L, and ffrench-Constant C (2016). Integrin signalling regulates the expansion of neuroepithelial progenitors and neurogenesis via Wnt7a and Decorin. Nat. Commun. 7, 10354. [PubMed: 26838601]

Lui JH, Hansen DV, and Kriegstein AR (2011). Development and evolution of the human neocortex. Cell 146, 18–36. [PubMed: 21729779]

Madisen L, Mao T, Koch H, Zhuo J, Berenyi A, Fujisawa S, Hsu Y-WA Iii, A. JG, Gu X, Zanella S, et al. (2012). A toolbox of Cre-dependent optogenetic transgenic mice for light-induced activation and silencing. Nat. Neurosci. 15, 793–802. [PubMed: 22446880]

dal Maschio M, Ghezzi D, Bony G, Alabastri A, Deidda G, Brondi M, Sato SS, Zaccaria RP, Di Fabrizio E, Ratto GM, et al. (2012). High-performance and site-directed in utero electroporation by a triple-electrode probe. Nat. Commun. 3, 960. [PubMed: 22805567]

Mizutani K, Yoon K, Dang L, Tokunaga A, and Gaiano N (2007). Differential Notch signalling distinguishes neural stem cells from intermediate progenitors. Nature 449, 351–355. [PubMed: 17721509]

Molyneaux BJ, Goff LA, Brettler AC, Chen H-H, Brown JR, Hrvatin S, Rinn JL, and Arlotta P (2015). DeCoN: Genome-wide Analysis of In Vivo Transcriptional Dynamics during Pyramidal Neuron Fate Selection in Neocortex. Neuron 85, 275–288. [PubMed: 25556833]

Nieuwenhuis J, and Brummelkamp TR (2018). The Tubulin Detyrosination Cycle: Function and Enzymes. Trends Cell Biol.

Nieuwenhuis J, Adamopoulos A, Bleijerveld OB, Mazouzi A, Stickel E, Celie P, Altelaar M, Knipscheer P, Perrakis A, Blomen VA, et al. (2017). Vasohibins encode tubulin detyrosinating activity. Science 358, 1453–1456. [PubMed: 29146869]

Nirschl JJ, Magiera MM, Lazarus JE, Janke C, and Holzbaur ELF (2016). α-Tubulin Tyrosination and CLIP-170 Phosphorylation Regulate the Initiation of Dynein-Driven Transport in Neurons. Cell Rep. 14, 2637–2652. [PubMed: 26972003]

Nowakowski TJ, Pollen AA, Sandoval-Espinosa C, and Kriegstein AR (2016). Transformation of the Radial Glia Scaffold Demarcates Two Stages of Human Cerebral Cortex Development. Neuron 91, 1219–1227. [PubMed: 27657449]

Pamula MC, Ti S-C, and Kapoor TM (2016). The structured core of human β tubulin confers isotype-specific polymerization properties. J. Cell Biol. 213, 425–433. [PubMed: 27185835]

Paturle-Lafanechere L, Manier M, Trigault N, Pirollet F, Mazarguil H, and Job D (1994). Accumulation of delta 2-tubulin, a major tubulin variant that cannot be tyrosinated, in neuronal tissues and in stable microtubule assemblies. J. Cell Sci. 107, 1529–1543. [PubMed: 7962195]

Peris L, Thery M, Fauré J, Saoudi Y, Lafanechère L, Chilton JK, Gordon-Weeks P, Galjart N, Bornens M, Wordeman L, et al. (2006). Tubulin tyrosination is a major factor affecting the recruitment of CAP-Gly proteins at microtubule plus ends. J. Cell Biol. 174, 839–849. [PubMed: 16954346]

Petros TJ, Bultje RS, Ross ME, Fishell G, and Anderson SA (2015). Apical versus Basal Neurogenesis Directs Cortical Interneuron Subclass Fate. Cell Rep. 13, 1090–1095. [PubMed: 26526999]

Pilaz L-J, Lennox AL, Rouanet JP, and Silver DL (2016). Dynamic mRNA Transport and Local Translation in Radial Glial Progenitors of the Developing Brain. Curr. Biol. 26, 3383–3392. [PubMed: 27916527]

Pilz G-A, Shitamukai A, Reillo I, Pacary E, Schwausch J, Stahl R, Ninkovic J, Snippert HJ, Clevers H, Godinho L, et al. (2013). Amplification of progenitors in the mammalian telencephalon includes a new radial glial cell type. Nat. Commun. 4, 2125. [PubMed: 23839311]

Qian X, Goderie SK, Shen Q, Stern JH, and Temple S (1998). Intrinsic programs of patterned cell lineages in isolated vertebrate CNS ventricular zone cells. Development 125, 3143–3152. [PubMed: 9671587]

Reillo I, and Borrell V (2012). Germinal zones in the developing cerebral cortex of ferret: ontogeny, cell cycle kinetics, and diversity of progenitors. Cereb. Cortex N. Y. N 1991 22, 2039–2054.

Rodriguez JA, and Borisy GG (1979). Experimental phenylketonuria: replacement of carboxyl terminal tyrosine by phenylalanine in infant rat brain tubulin. Science 206, 463–465. [PubMed: 574315]

Rogowski K, van Dijk J, Magiera MM, Bosc C, Deloulme J-C, Bosson A, Peris L, Gold ND, Lacroix B, Grau MB, et al. (2010). A Family of Protein-Deglutamylating Enzymes Associated with Neurodegeneration. Cell 143, 564–578. [PubMed: 21074048]

Roll-Mecak A (2019). How cells exploit tubulin diversity to build functional cellular microtubule mosaics. Curr. Opin. Cell Biol. 56, 102–108. [PubMed: 30466050]

Romaniello R, Arrigoni F, Fry AE, Bassi MT, Rees MI, Borgatti R, Pilz DT, and Cushion TD (2018). Tubulin genes and malformations of cortical development. Eur. J. Med. Genet.

Sahara S, and O'Leary DD (2009). Fgf10 regulates transition period of cortical stem cell differentiation to radial glia controlling generation of neurons and basal progenitors. Neuron 63, 48–62. [PubMed: 19607792]

Sahara S, Kawakami Y, Izpisua Belmonte JC, and O'Leary DDM (2007). Sp8 exhibits reciprocal induction with Fgf8 but has an opposing effect on anterior-posterior cortical area patterning. Neural Develop. 2, 10.

Sekine K, Ohuchi H, Fujiwara M, Yamasaki M, Yoshizawa T, Sato T, Yagishita N, Matsui D, Koga Y, Itoh N, et al. (1999). Fgf10 is essential for limb and lung formation. Nat Genet 21, 138–141. [PubMed: 9916808]

Shimojo H, Ohtsuka T, and Kageyama R (2008). Oscillations in Notch Signaling Regulate Maintenance of Neural Progenitors. Neuron 58, 52–64. [PubMed: 18400163]

Stanchi F, Corso V, Scannapieco P, Ievolella C, Negrisolo E, Tiso N, Lanfranchi G, and Valle G (2000a). TUBA8: A New Tissue-Specific Isoform of α-Tubulin That Is Highly Conserved in Human and Mouse. Biochem. Biophys. Res. Commun. 270, 1111–1118. [PubMed: 10772959]

Stanchi F, Corso V, Scannapieco P, Ievolella C, Negrisolo E, Tiso N, Lanfranchi G, and Valle G (2000b). TUBA8: A New Tissue-Specific Isoform of α-Tubulin That Is Highly Conserved in Human and Mouse. Biochem. Biophys. Res. Commun. 270, 1111–1118. [PubMed: 10772959]

Stancik EK, Navarro-Quiroga I, Sellke R, and Haydar TF (2010). Heterogeneity in Ventricular Zone Neural Precursors Contributes to Neuronal Fate Diversity in the Postnatal Neocortex. J. Neurosci. 30, 7028–7036. [PubMed: 20484645]

Tan X, Liu WA, Zhang X-J, Shi W, Ren S-Q, Li Z, Brown KN, and Shi S-H (2016). Vascular Influence on Ventral Telencephalic Progenitors and Neocortical Interneuron Production. Dev. Cell 36, 624–638. [PubMed: 27003936]

Taverna E, Götz M, and Huttner WB (2014). The Cell Biology of Neurogenesis: Toward an Understanding of the Development and Evolution of the Neocortex. Annu. Rev. Cell Dev. Biol. 30, null.

Tyler WA, and Haydar TF (2013). Multiplex Genetic Fate Mapping Reveals a Novel Route of Neocortical Neurogenesis, Which Is Altered in the Ts65Dn Mouse Model of Down Syndrome. J. Neurosci. 33, 5106–5119. [PubMed: 23516277]

Vemu A, Atherton J, Spector JO, Moores CA, and Roll-Mecak A (2017). Tubulin isoform composition tunes microtubule dynamics. Mol. Biol. Cell 28, 3564–3572. [PubMed: 29021343]

Vitali I, Fièvre S, Telley L, Oberst P, Bariselli S, Frangeul L, Baumann N, McMahon JJ, Klingler E, Bocchi R, et al. (2018). Progenitor Hyperpolarization Regulates the Sequential Generation of Neuronal Subtypes in the Developing Neocortex. Cell 174, 1264–1276.e15. [PubMed: 30057116]

Yap K, Mukhina S, Zhang G, Tan JSC, Ong HS, and Makeyev EV (2018). A Short Tandem Repeat-Enriched RNA Assembles a Nuclear Compartment to Control Alternative Splicing and Promote Cell Survival. Mol. Cell 72, 525–540.e13. [PubMed: 30318443]

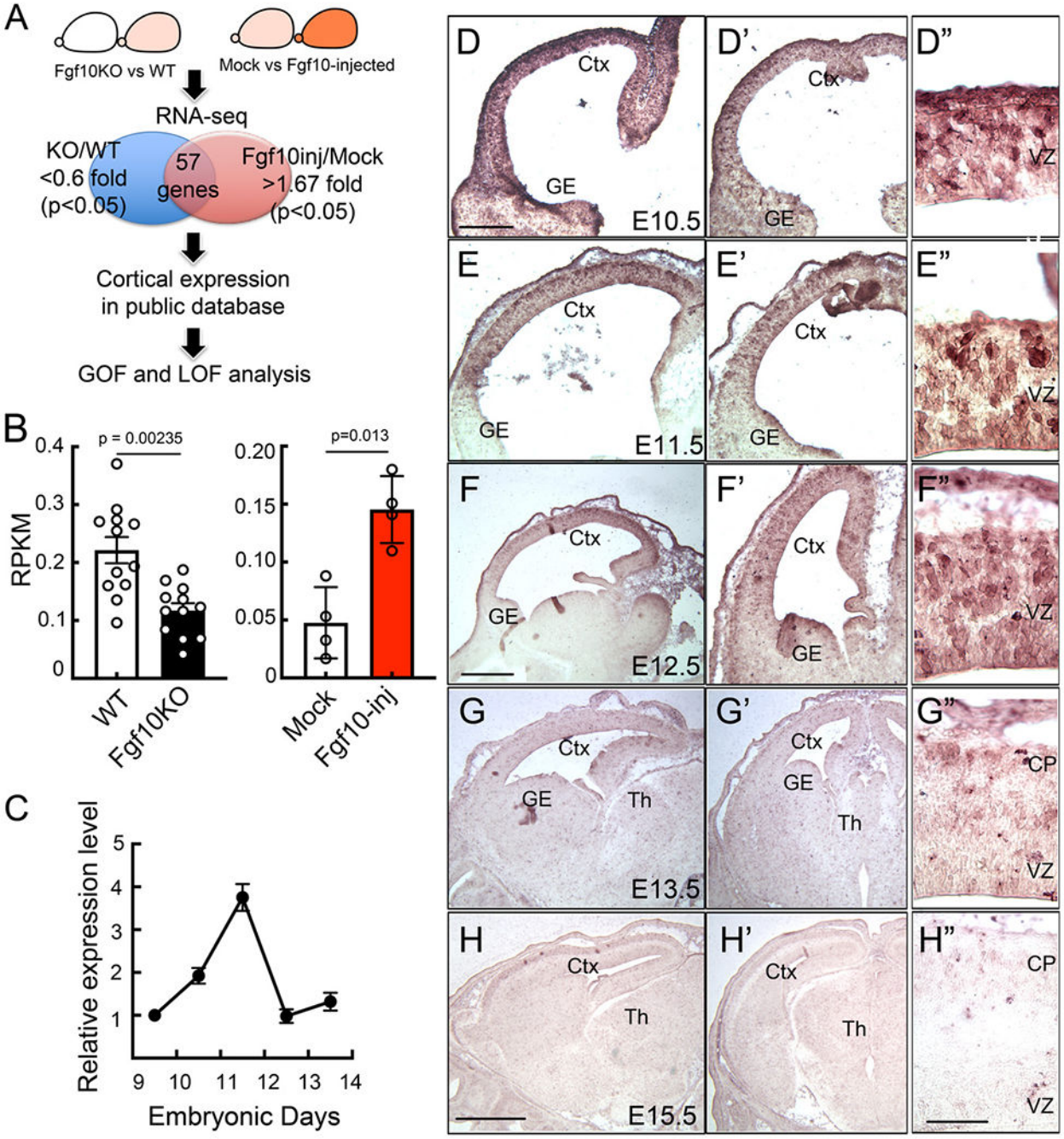

Figure 1. Tuba8, a downstream of Fgf10 signalling, is expressed transiently at the onset of mouse cortical neurogenesis

(A) Transcriptome analysis, comparing E11.5 Fgf10KO cortices to WT (Loss-of-function, LOF), and Fgf10 protein-injected cortices to mock injections (Gain-of-function, GOF). Genes downregulated >1.67-fold in Fgf10KO cortices and upregulated >1.67-fold in Fgf10-injected cortices compared to corresponding controls ($p<0.05$) were shortlisted for further analyses. (B) RNAseq data showing a 1.92-fold decrease in the expression of Tuba8 in Fgf10KO cortices (n=12) and a 3.05-fold increase in Fgf10-injected cortices (n=4). (C) Tuba8 expression levels in E9.5 to E13.5 mouse cortices analyzed by RT-qPCR. Tuba8

mRNA level peaks at E11.5 (n=4). Data were normalized by GAPDH expression, followed by the value at E9.5 and are represented as mean ± SEM. (D-H") Tuba8 expression in sagittal (D-H) or coronal (D'-H') sections of developing mouse forebrains analyzed by *in situ* hybridization at the ages indicated. D"-H" indicate a higher magnification of D-H, respectively. Tuba8 expression is strong in a subset of progenitors that reside in the dorsal cortex between E10.5 to E12.5, but is downregulated from E13.5 onwards. Ctx: cortex, GE: ganglionic eminence, Th: thalamus, VZ: ventricular zone, CP: cortical plate. Scale bars: 250 μm (D, E, D', E'), 0.5 mm (F, G, F', G'), 1 mm (H, H'), 50 μm (D"-G"), 100 μm (H").

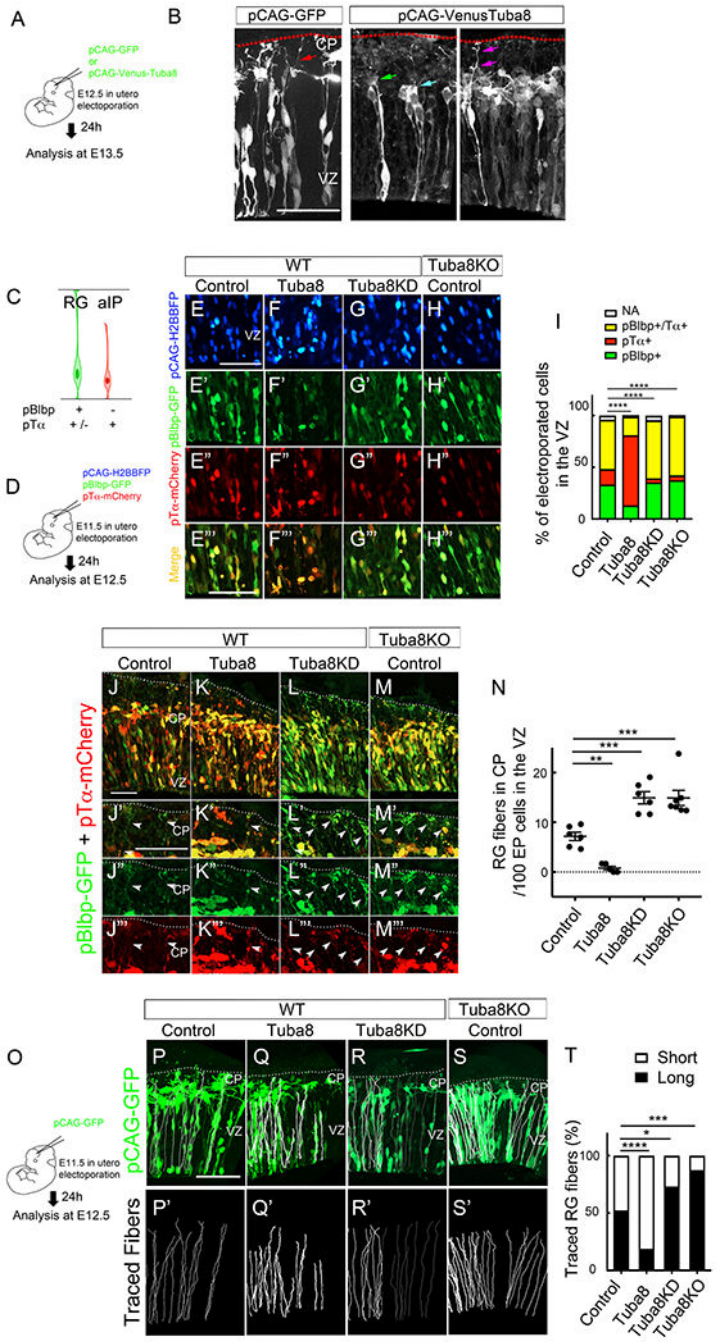

Figure 2. Tuba8 induces aIP fate in the developing mouse cortex

(A) *In utero* electroporation strategy used in (B).

(B) E13.5 cortices electroporated with a Venus-Tuba8 fusion protein or a GFP control at E12.5. The GFP signal is distributed throughout the entire RG, including the fibers attached to the basal lamina (left panel, red arrow). In contrast, the Venus-Tuba8 signal is detected in RG fibers that terminate at the border between the VZ and CP (middle panel, green arrow) and in cells with thin bifurcated or no basal fibers (light blue arrow). A few cases were detected where highly branched basal processes appeared to contact the basal lamina (right

panel, magenta arrows). (C) A diagram representing the difference between RGs and aIPs. (D) *In utero* electroporation strategy employed in (E-N). (E-I) Quantification of progenitor cells in the VZ of E12.5 cortices electroporated with pBlbp-GFP (E'-H') and pTα-mCherry (E"-H"), including merged images of two promoters (E"'-H"'). Co-electroporated with the constructs indicated; Tuba8 (F-F"') and Tuba8 knockdown (Tuba8KD) (G-G"') were overexpressed in the WT, and control vectors in Tuba8KO cortices (H-H"'). Total number of electroporated cells monitored by the expression of H2BBFP driven by the CAG promoter (E-H). (I) Counting of green single positive cells as pBlbp+, red single positive cells as pTα+, and double positive cells as pBlbp+/pTα+ cells. Overexpression of Tuba8 increases the fraction of pTα+ cells compared to the control, while knockdown and knockout of Tuba8 both decrease the fraction of pTα+ cells. Chi-square test (I), ****$p < 0.0001$. (J-N) Quantification of RG fibers labelled by pBlbp-GFP and pTα-mCherry in the CP of E12.5 cortices co-electroporated with control (J-J"'), Tuba8 (K-K"'), Tuba8KD constructs (L-L"'), or in Tuba8KO cortices electroporated with a control vector (M-M"'). In comparison to the control (J-J"'), there are fewer RG fibers in the CP of Tuba8 electroporated cortices (K-K"), while those electroporated with the Tuba8KD construct (L-L"') or those of Tuba8KO mice (M-M"') showed an increased number of RG fibers (arrowheads). Dotted lines indicate the border of the cortical plates and basal membranes. The number of RG fibers was normalized to the number of electroporated cells in the VZ (E-H, N). Data are represented as mean ± SEM. One-way ANOVA (N). **$p < 0.01$, p***< 0.001. The intensity of red channel in J"'-M"' is increased for the better visualization of the RG fibers. (O) An illustration of the *in utero* electroporation strategy employed in (P-T). (P-T) Quantification of RG fibers labelled by pCAG-GFP. The projections of GFP+ progenitors co-electroporated with control (P, P'), Tuba8 (Q, Q'), or Tuba8KD constructs (R-R'), or those in Tuba8KO mice (S, S') were traced using Simple Neurite Tracer to track their trajectories from the apical to the basal membrane in 100 μm sections. Maximum projection images with their traces (P-S) and traced images (P'-S') are shown. (T) Tuba8 overexpressing cortices contain more short progenitors with fibers that end in the middle of the cortex, while those electroporated with the Tuba8KD construct or Tuba8KO cortices have more progenitors whose fibers contact the basal lamina. chi-square test (T), *$p < 0.05$, ***$p < 0.001$, ****$p < 0.0001$.
VZ: ventricular zone, CP: cortical plate. Scale bars: 50 μm (B), 50 μm (E-H"'), 50 μm (J'-M"'). (J-M), 100 μm (M-P').

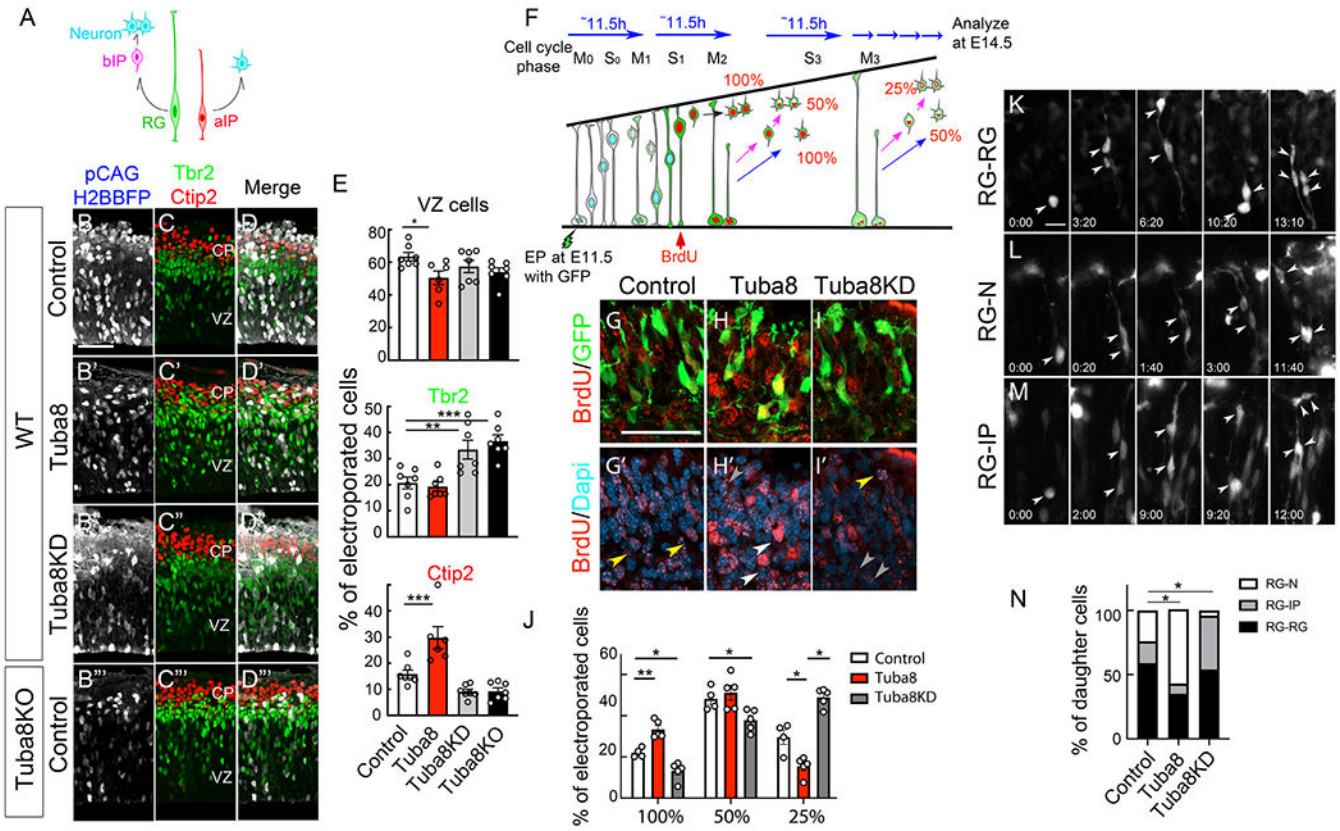

Figure 3. Tuba8 promotes direct neurogenesis in the developing mouse cortex

(A-E) Direct neurogenesis is induced by Tuba8. WT cortices electroporated with a pCAG-H2BBFP vector together with control (B-D), Tuba8 (B'-D'), or Tuba8KD (B"-D") constructs at E11.5, or Tuba8KO cortices with a control vector (B"'-D"') were analyzed 24 hours post-electroporation by immunostaining against Tbr2 and Ctip2. The number of Ctip2+ cells increased in cortices electroporated with Tuba8 in comparison to control cortices. The number of Tbr2+ cells increased in Tuba8KD cortices and Tuba8KO cortices, both of which showed no significant differences in the number of Ctip2+ cells when compared to their respective controls. One-way ANOVA (E). *p < 0.05, **p< 0.01, ***p <0.001. VZ: ventricular zone, CP: cortical plate.

(F-J) Estimation of direct and indirect neurogenesis in Tuba8-manipulated progenitors by combining GFP and BrdU retention. BrdU was injected 3 hours before the 2nd mitotic division (M2). Postmitotic cells with the highest BrdU signal (100%) were either generated directly from apical progenitors at M2 or from bIPs following their 1st mitotic division (M1), while those with 50% BrdU signal intensity were assumed to be generated via indirect neurogenesis. (G-I') GFP and BrdU double staining images of E14.5 cortical plates electroporated with pCAG-GFP vector together with control (G, G"), Tuba8 (H, H'), or Tuba8KD (I, I") vector. Representative examples of 100%, 50%, and 25% cells are indicated by white, yellow, and grey arrowheads, respectively. Data in E and J are represented as mean ± SEM. In comparison to controls, the fraction of the 100% BrdU cells is increased in Tuba8 overexpressing cortices at the expense of the 25% cells, while Tuba8KD induced an opposite

effect with a reduction of 100% cells and an increase in 25% cells. Two-way ANOVA (J). *p < 0.05, **p< 0.01, ***p <0.001.

(K-N) Time-lapse imaging of Tuba8 manipulated progenitors from the M-phase. Arrowheads indicate the progenies from the starting cells. Tuba8 overexpression increases the fraction of RG-N divisions, while knockdown increases RG-bIP divisions in comparison to controls. Chi-square test (N). *p < 0.05. Scale bars: 50 μm (B-D”’), 50 μm (G-I’). 20 μm (K-M).

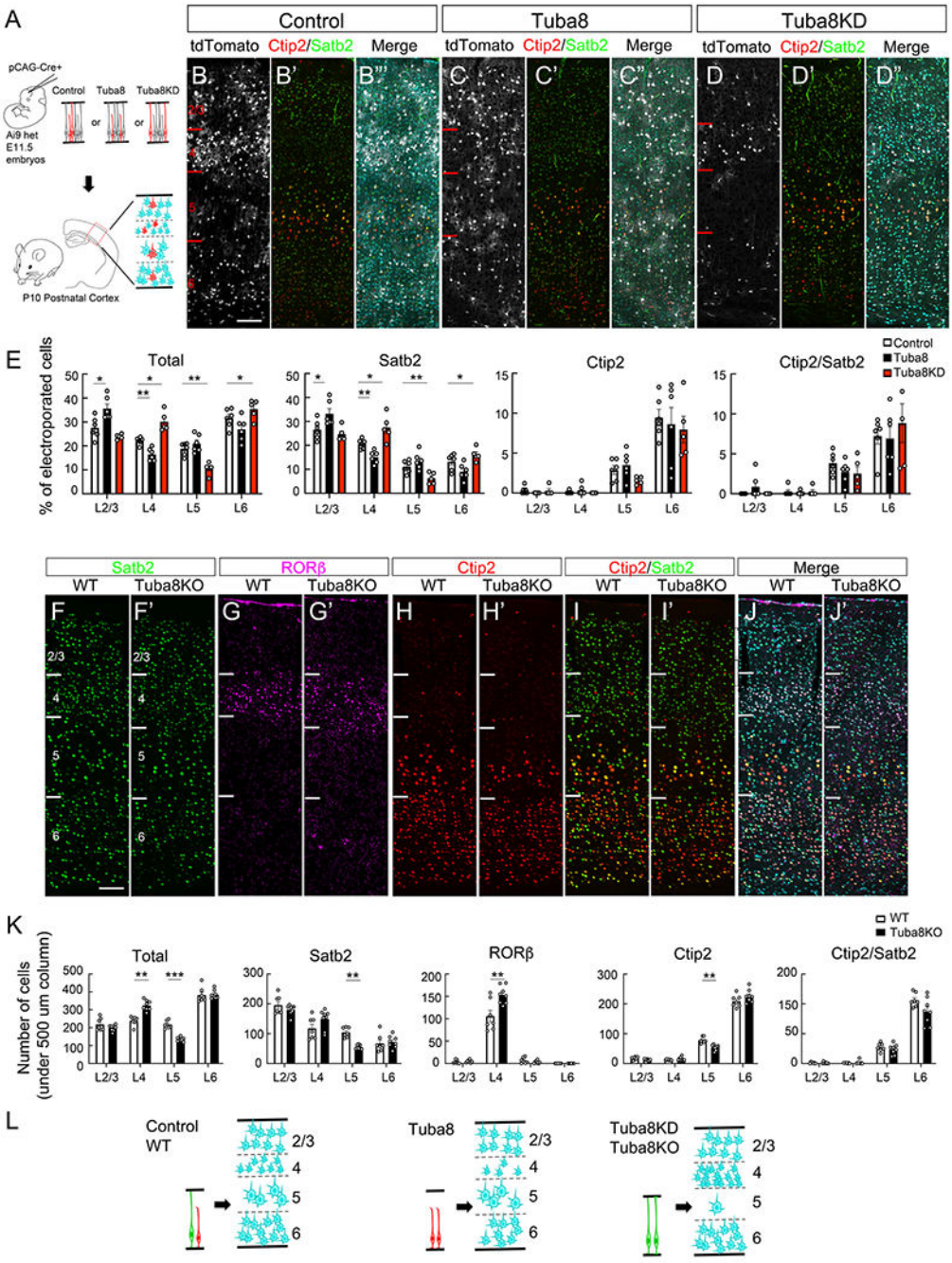

Figure 4. Manipulation of Tuba8 levels in cortical progenitors results in the distinct lineage outcomes in the postnatal cortex

(A-E) Lineage tracing study of Tuba8-manipulated progenitors. (A) *In utero* electroporation strategy used in (B-D"). pCAG-Cre were co-electroporated with the plasmids indicated into E11.5 Ai9 heterozygote embryos and harvested by P10.

(B-E) Layer distributions of tdTomato+ cells in the P10 cortex electroporated with pCAG-Cre together with control (B-B"), Tuba8 (C-C") or Tuba8KD construct (D-D"). Sections were stained against Ctip2 (red) and Satb2 (green) to distinguish neuronal subtypes. tdTomato+ cells were counted per layer and Ctip2/Satb2 cells were normalized by the total

number of tdTomato+ cells excluding glial cells. Tuba8 overexpression increases the fraction of Satb2+ L2 and L5 neurons with a reduction in L4 neurons, while knockdown increases Satb2+ L4 and L6 neurons with a reduction in L5 neurons (E). Two-way ANOVA (E). *$p < 0.05$, **$p < 0.01$.

(F-K) Quantification of layer neurons in the P16 postnatal cortex of Tuba8KO mice showing an increase in L4 neurons labelled by RORβ+(magenda)/Satb2+ and a reduction in Satb2+ L5 neurons, similar to the Tuba8KD phenotype, and L5 Ctip2+ neurons. Data in E and K are represented as mean ± SEM. Two-way ANOVA (K). **$p < 0.01$, ***$p < 0.001$. Scale bars: 100 μm (B-D”), 100 μm (F-J’). (L) A summary diagram of neuronal distribution in Tuba8-manipulated cortices.

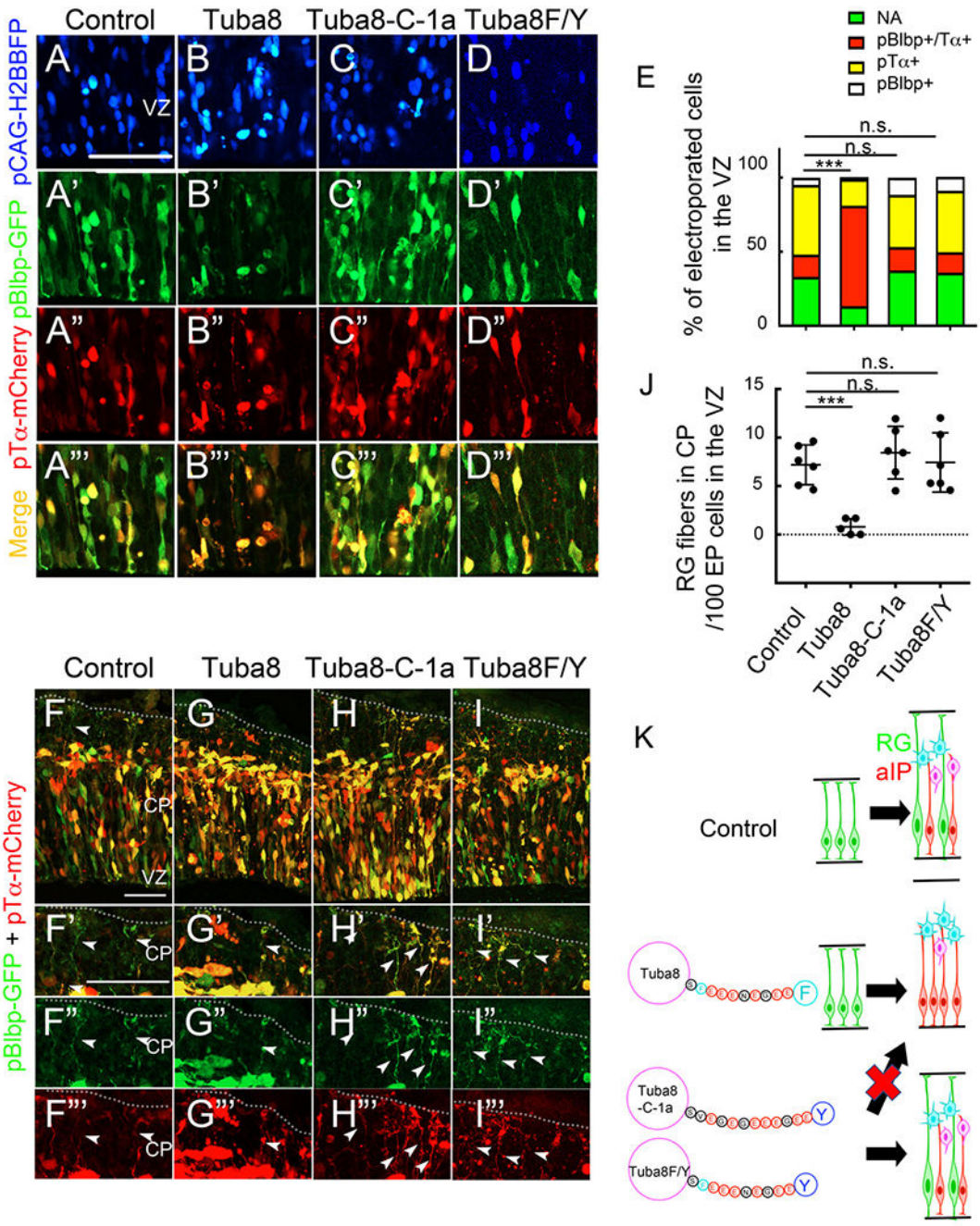

Figure 5. Tyrosine substitution of phenylalanine in Tuba8 abolishes aIP differentiation activity, but is not sufficient to induce supernumerary RG fibers

(A-E) Quantification of pBlbp-GFP and pTα-mCherry positive cells in the VZ of E12.5 cortices electroporated with control (A-A"'), Tuba8 (B-B"'), Tuba8-C-1a (C-C"'), or Tuba8F/Y constructs (D-D"'). Chi-square test (E). ***p < 0.001. (F-I"', J) Quantification of RG fibers in the CP of cortices electroporated with control (F-F"'), Tuba8 (G-G"'), Tuba8-C-1a (H-H"'), or Tuba8F/Y constructs (I-I"'). Data are represented as mean ± SEM. One-way ANOVA (J). ***p < 0.001. Scale bars: 50 μm (A-D'''), 50 μm (F-I'''). (K) A schematic diagram of tubulin mutants with Y or F in their C-terminal tails, and their effect on RG-aIP

differentiation. Progenitors expressing Tuba8 mutants with Y residues in their C-terminals (Tuba8F/Y and Tuba8-C-1a) are no longer biased towards aIP fate. Overexpression of these mutants is, however, insufficient to induce extra RG fibers, as observed in Tuba8KD or Tuba8KO cortices. Control and Tuba8 overexpression data from Figure 2 are included here for comparison between Tuba8 and Tuba8 mutant constructs.

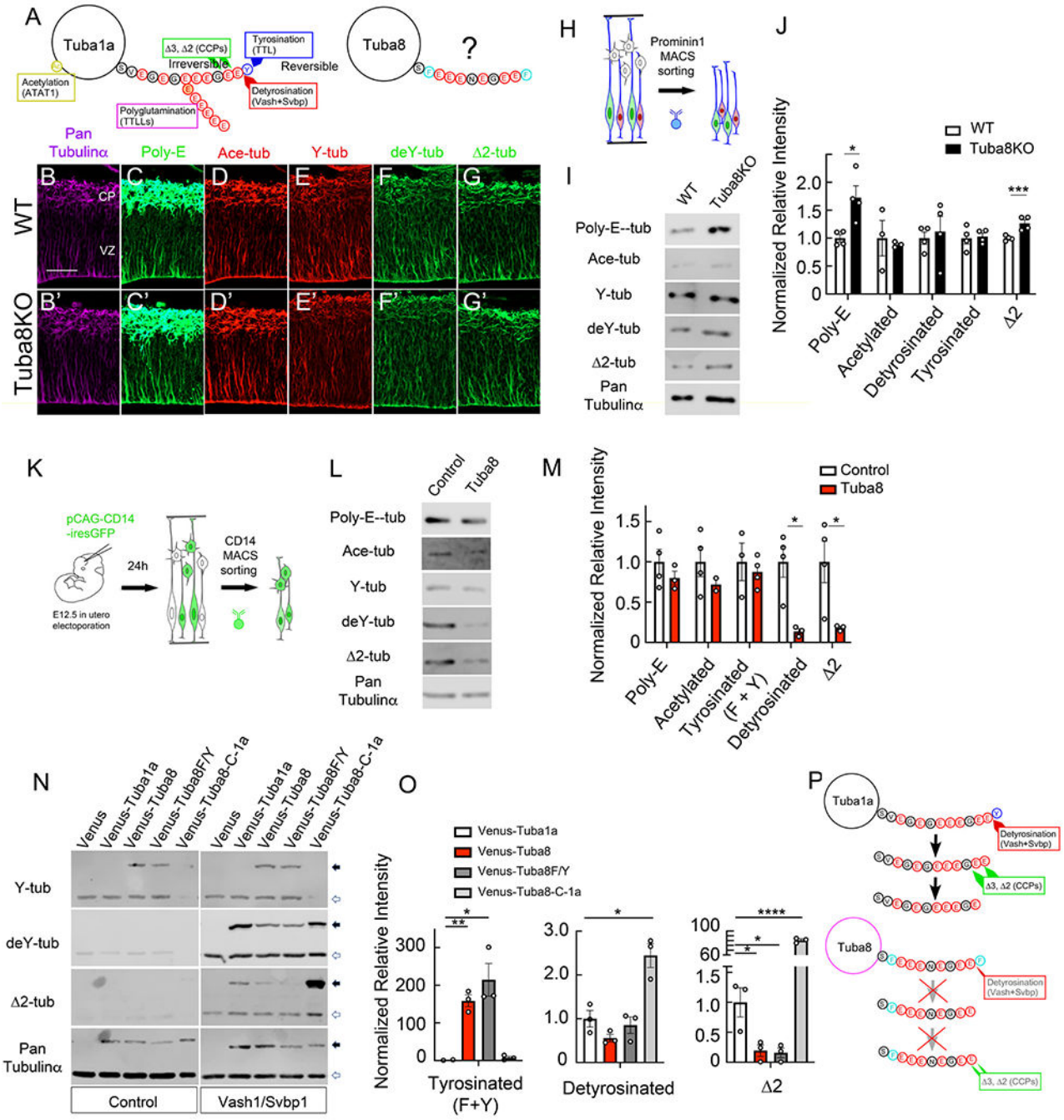

Figure 6. Tuba8 C-terminal tail is immune to detyrosination and Δ2 cleavage

(A) A diagram of the C-terminal tail amino acid sequence of Tuba1a and Tuba8, and major posttranslational modification sites. (B-G') Immunostaining of WT (B-G) and Tuba8KO (B'-G') cortices at E13.5 with antibodies against tubulin PTMs, namely poly-glutamination (poly-E, C, C'), acetylation (Ace-tub, D, D'), tyrosination (Y-tub, E, E'), detyrosination (de-Y-tub, F, F'), and Δ2-tubulin modifications (Δ2-Tub, G, G'). Sections were co-stained with a pan-tubulin-α antibody (B, B'). Scale bar: 50 μm. (H-J) Quantification of tubulin PTMs in Tuba8KO progenitors. Protein extracts from Prominin-1-sorted progenitors from WT or

Tuba8KO E13.5 cortices were stained with antibodies indicated. The intensity was normalized by pan-tubulin-α expression. Student's t-test (J). *p < 0.05, **p < 0.01. (K-M) Quantification of tubulin PTMs in cortices electroporated with control or Tuba8 constructs together with CD14. Protein extracts from CD14-sorted cells were stained against the PTMs indicated. Tuba8 overexpression reduced the levels of detyrosination and Δ2 modifications (M). Student's t-test (M). *p < 0.05. (N, O) Quantification of PTMs in in Venus-tubulin-α. Protein extracts from HEK293 cells transfected with control, Tuba1a, Tuba8, Tuba8F/Y, or Tuba8-C-1a constructs tubulin with or without Vash1/Svbp1 overexpression were stained with antibodies against tyrosinated, detyrosinated, or Δ2-tubulin. The amount of endogenous (55 kDa, white arrows) and Venus-fused tubulins (95 kDa, black arrows) were normalised by pan-tubulin-α expression. In the presence of Vash1/Svbp1, both Tuba8 and the F/Y mutant forms maintained high levels of tyrosine or phenylalanine at their C-termini, and could not be cleaved into Δ2-tubulin. This indicates that the C-terminal tail of Tuba8 is immune to detyrosination and Δ2-tubulin cleavage (O, P). Data in I, L and O are represented as mean ± SEM. Student's t-test with BH correction (O). *p < 0.05, **p < 0.01, ****p < 0.0001.

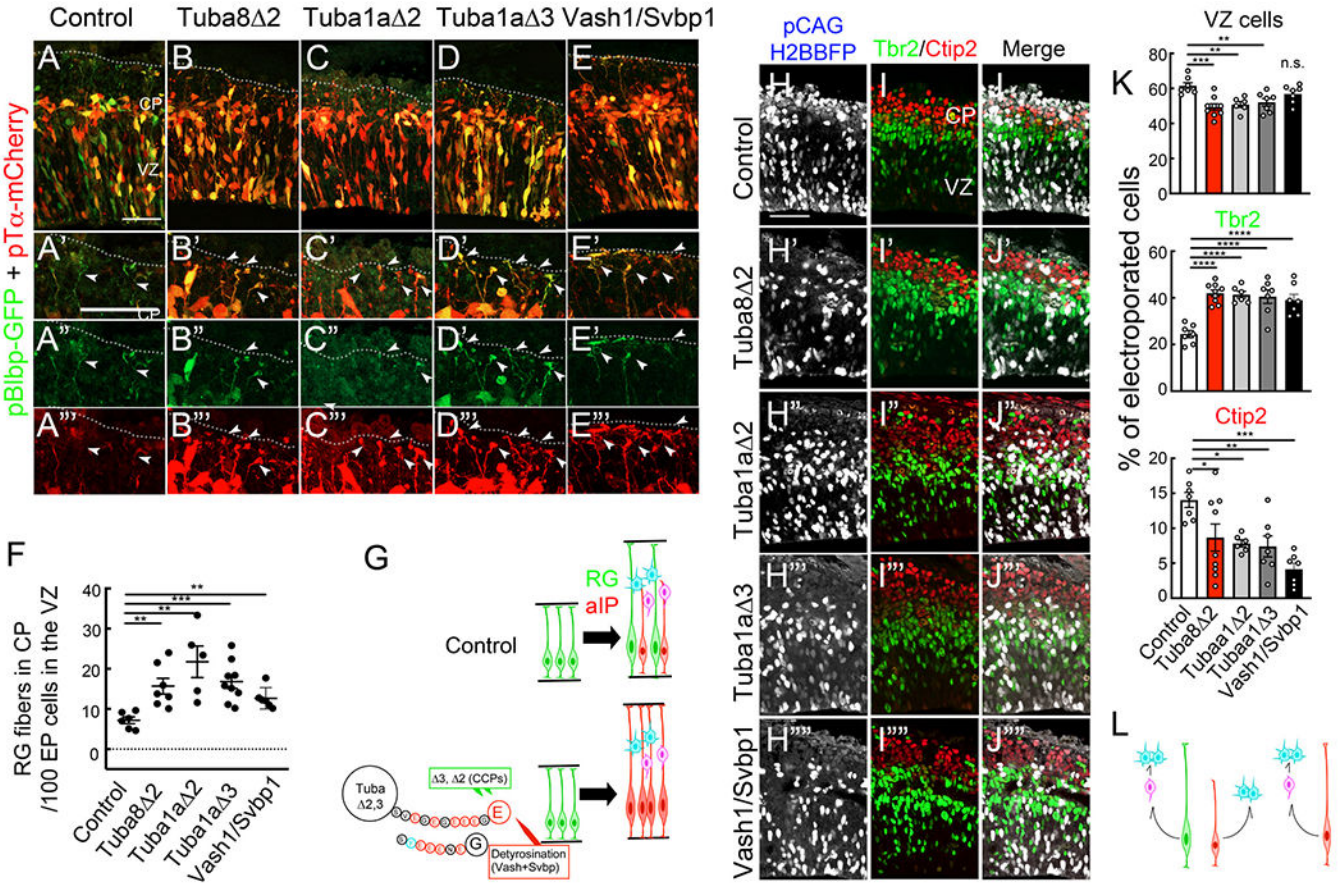

Figure 7. Δ2/3-tubulin induces supernumerary basal RG fibers and promotes indirect neurogenesis

(A-F) Quantification of pBlbp-GFP and pTα-mCherry positive RG fibers in E12.5 cortices co-electroporated with Tuba8Δ2 (B-B”’), Tuba1aΔ2 (C-C”’), Tuba1aΔ3 (D-D”’), or Vash1/Svbp1 constructs (E-E”’). Overexpression of all TubaΔ2/3 mutants or Vash1/Svbp1, which facilitates Δ2-cleavage of endogenous tubulins, induces supernumerary RG fibers, as observed in Tuba8KD and KO cortices (G). One-way ANOVA (F). **p <0.01. (H-L) Quantification of Tbr2+ and Ctip2+ cells in cortices electroporated with control (H-J), Tuba8Δ2 (H’-J’), Tuba1aΔ2 (H”-J”), or Tuba1aΔ3 (H’”-J”’), or Vash1/Sbvp1 (H””-J””) together with pCAG-H2BBFP. The fraction of Tbr2+ cells co-electroporated with Δ2/3-tubulin and Vash1/Svbp1 constructs increased at the expense of Ctip2+ cells compared to controls, suggesting Δ2 and 3-tubulins facilitate indirect neurogenesis (L). Control data from Figure 2 and 3 is included here for comparison. Data in F and K are represented as mean ± SEM. One-way ANOVA (K). *p < 0.05, **p < 0.01, ***p< 0.001, ****p <0.0001. Scale bars: 50 μm (A-E””), 50 μm (H-J’’’’).

Key Resources Table

REAGENT or RESOURCE	SOURCE	IDENTIFIER
Antibodies		
Mouse anti-Arl13b	NeuroMab (UC Davis)	Cat#75-287 RRID: AB_2341543
Rabbit anti-γ-Tubulin	Sigma-Aldrich	Cat# T5192, AB_261690
Rabbit anti-phospho-histone H3	Cell signaling technology	Cat# 53348 AB_2799431
Rabbit anti-Tbr1	Merck-Millipore	Cat# AB_2261 AB_10615497
Rabbit anti-Satb2	Abcam	Cat# AB_92446 AB_10563678
Mouse anti-Satb2	Abcam	Cat# AB_51502 AB_882455
Mouse anti-RORβ	R&D systems	Cat# PP-N7927-00 AB_1964364
DM1A	Thermo Fisher Scientific	Cat# MA1-90201 AB_1954824
Rat anti-Ctip2	Abcam	Cat # ab18465 AB_2064130
Chicken anti-Tbr2	Merck-Millipore	Cat# AB15894, AB_10615604
Rabbit anti-Tbr2	Abcam	Cat# ab183991, AB_2721040
Rabbit anti-Pax6	Covance	Cat# PRB-278P-100, AB_291612
Rat anti-Nestin (RC2)	DSHB	Cat# Rat-401 AB_2235915
Guinea pig anti-tagRFP antibody	Kerafast	EMU107
Chick anti-GFP antibody	Thermo Fisher Scientific	Cat# A10262 AB_2534023
Rabbit anti-Polyglutamate chain (polyE) pAb (IN105) antibody	AdipoGen	Cat# AG-25B-0030 AB_2490540
Mouse anti- acetylated alpha Tubulin (6-11B-1)	Santa Cruz Biotechnology	Cat# sc-23950 AB_628409
Rabbit anti- Detyrosinated alpha Tubulin antibody	Abcam	Cat#48389 AB_869990
Rat anti-tyrosinated tubulin (YL1/2)	Santa Cruz Biotechnology	Cat# MA1-34617
Rabbit anti-Δ2 tubulin	Abcam	Cat#ab106658 AB_10861939
Rat Anti-Mouse CD29 Clone 9EG7	BD bioscience	Cat #550531 AB_393729
Guinea pig anti-tagRFP	Kerafast	Cat#EMU108
Guinea pig anti-Glutamate Transporter, Glial antibody	Millipore	Cat#AB1783 AB_90949
Rabbit anti-Brain lipid binding protein antibody	Abcam	Cat#ab183991 AB_2721040
Rat anti-Nestin antibody	BD Biosciences	Cat# 556309 AB_396354

REAGENT or RESOURCE	SOURCE	IDENTIFIER
Donkey Anti-Mouse IgG (H+L) Antibody, Alexa Fluor 405 Conjugated	Thermo Fisher Scientific	Cat # A-31553 AB_221604
Donkey Anti-Mouse IgG (H+L) Antibody, Alexa Fluor 488 Conjugated	Thermo Fisher Scientific	Cat # A-21202 AB_141607
Donkey Anti-Mouse IgG (H+L) Antibody, Alexa Fluor 568 Conjugated	Thermo Fisher Scientific	Cat # A10037 AB_2534013
Donkey Anti-Mouse IgG (H+L) Antibody, Alexa Fluor 647 Conjugated	Thermo Fisher Scientific	Cat # A-31571 AB_162542
Donkey Anti-Rabbit IgG (H+L) Antibody, Alexa Fluor 488 Conjugated	Thermo Fisher Scientific	Cat # A-21206 AB_2535792
Donkey Anti-Rabbit IgG (H+L) Antibody, Alexa Fluor 568 Conjugated	Thermo Fisher Scientific	Cat # A10042 AB_2534017
Donkey Anti-chicken IgY (H+L) Antibody, Alexa Fluor 488 Conjugated	Jackson Laboratory	Cat # 703-545-155 AB_2340375
Goat Anti-Rat IgG (H+L) Antibody, Alexa Fluor 568 Conjugated	Thermo Fisher Scientific	Cat # A-11077 AB_2534121
Goat Anti-Guinea pig Alexa Fluor 405 Conjugated	Abcam	Cat # ab175678
Goat Anti-Mouse IgG (H+L) Antibody, Alexa Fluor 405 Conjugated	Thermo Fisher Scientific	Cat # A-31553 AB_221604
Donkey Anti-Mouse IgG (H+L) Antibody, Alexa Fluor 488 Conjugated	Thermo Fisher Scientific	Cat # A-21202 AB_141607
Donkey Anti-Mouse IgG (H+L) Antibody, Alexa Fluor 568 Conjugated	Thermo Fisher Scientific	Cat # A10037 AB_2534013
Donkey Anti-Mouse IgG (H+L) Antibody, Alexa Fluor 647 Conjugated	Thermo Fisher Scientific	Cat # A-31571 AB_162542
Donkey Anti-Rabbit IgG (H+L) Antibody, Alexa Fluor 488 Conjugated	Thermo Fisher Scientific	Cat # A-21206 AB_2535792
Donkey Anti-Rabbit IgG (H+L) Antibody, Alexa Fluor 568 Conjugated	Thermo Fisher Scientific	Cat # A10042 AB_2534017
Anti-Digoxigenin-AP, Fab fragments	Sigma	Cat # 1093274910
Goat anti-Rabbit IgG (Heavy&Light Chain) Antibody	Li-COR	Cat # P/N: 926-68073 AB_10954442
Goat anti-Mouse IgG (Heavy&Light Chain) Antibody	Li-COR	Cat # P/N: 926-32210 AB_621842
Goat anti-Rat IgG (Heavy&Light Chain) Antibody	Li-COR	Cat # P/N: 926-68076 AB_10956590
Kit		
RNeasy Micro Kit	QIAGEN	Cat # 74004
RevertAid First Strand DNA Synthesis Kit	Thermo Fisher Scientific	Cat # K1621
Expand Long Template PCR System	Sigma	Cat # 11681834001
Anti-Prominin-1 MicroBeads, mouse	Miltenyi Biotech	Cat # 130-092-333
CD14 MicroBeads, human	Miltenyi Biotech	Cat # 130-050-201
MS Columns	Miltenyi Biotech	Cat # 130-042-201
Oligonucleotides		
Oligonucleotides	Listed in Supplemental Table 3	Integrated DNA Technologies
Proteins		
Recombinant Fgf10	R&D systems	Cat # 6224-FG-025

REAGENT or RESOURCE	SOURCE	IDENTIFIER
Deposited Data		
RNA sequencing of E11.5 cortices from WT and Fgf10null mice		ArrayExpress accession: E-MTAB-8279
Experimental Models: Cell Lines		
HEK293 cell line		Beatriz Rico Lab
Experimental Models: Organisms/Strains		
Mouse: CD-1	Charles River, UK, Ltd	Strain code 022
Mouse: Tuba8KO	The Jackson Laboratory	Mouse strain datasheet: 029406
Mouse: Fgf10 Flox	In this study	
Mouse: CAG-Cre	The Jackson Laboratory	Mouse strain datasheet: 006054, B6.C-Tg(CMV-cre)1Cgn/J
Mouse: C57BL6/J	The Jackson Laboratory	Mouse strain datasheet: 000664
Mouse: Ai9	The Jackson Laboratory	Mouse strain datasheet: 007909, B6.Cg-Gt(ROSA)26Sor$^{tm9(CAG-tdTomato)Hze}$/J
Recombinant DNA		
pCAG-Tuba8	This paper	
pCAG-H2BtagBFP-Tuba8 miR-RNAi	This paper	
pCAG-Venus-Tuba8	This paper	
pCAG-H2BtagBFP	This paper	
pCAG-GFP	(Sahara et al., 2007)	
pBlbp-GFP	(Anthony et al., 2004)	
pTα-GFP	(Gal et al., 2006)	
pTα-mCherry	This paper	
pCAG-Cre	(Sahara et al., 2007)	
pCAG-Tuba1a	This paper	
pCAG-CD14-iresGFP	This paper	
pCAG-Tuba8F/Y	This paper	
pCAG-Tuba8-C-1a	This paper	
pCAG-Tuba8Δ2	This paper	
pCAG-Tuba1aΔ2	This paper	
pCAG- Tuba1aΔ3	This paper	
pCAG-Vash1	This paper	
pCAG-Svbp1	This paper	
pCAG-loxPSTOPloxP-ZsGreen	Addgene 51269	
Software and Algorithms		
Fiji	Fiji	https://imagej.nih.gov/ij/
Prism	Graphpad software	https://www.graphpad.com
ZEN	Carl Zeiss	https://www.zeiss.com/microscopy
Photoshop	Adobe systems	https://www.adobe.com/products/photoshop.html
Canvas Draw for Mac	Canvas GFX, Inc	https://www.canvasgfx.com
R	The R Foundation	https://www.r-project.org/

REAGENT or RESOURCE	SOURCE	IDENTIFIER
LI-COR Image Studio	LI-COR Biosciences	https://www.licor.com/bio/products/software/image_studio/